Cell-Free UAV Networks with Wireless Fronthaul: Analysis and Optimization

Carles Diaz-Vilor, Angel Lozano, and Hamid Jafarkhani barakhani

Abstract

The use of uncrewed aerial vehicles (UAVs) in cell-free networks is poised to unleash a number of new opportunities to further improve wireless networks. However, cell-free UAV networks present major challenges related to the wireless nature of access and fronthaul links. This manuscript studies the uplink of cell-free systems where users connect to UAVs, the latter devices forwarding the information to a processing point through imperfect wireless fronthaul links. Three multiple access alternatives are considered for the fronthaul, namely frequency division multiples access, spatial division multiple access, and combinations thereof. Deterministic equivalent expressions for the spectral efficiency under these fronthaul schemes and minimum mean-square error reception are derived. Then, the optimization subproblems of (a) the 3D deployment of the UAVs, (b) the user transmit powers, and (c) the UAV transmit powers, are investigated. The joint optimization of these subproblems yields superior performance, with the 3D deployment being the main source of improvement.

Index Terms

Cell-Free, UAV, fronthaul, FDMA, SDMA, deployment optimization, power optimization

I. INTRODUCTION

The race towards 6G wireless networks has begun and many ideas are under investigation [1], with uncrewed aerial vehicles (UAVs) as a potential game changer. Indeed, the inclusion of UAVs in wireless networks, and in particular their deployment as flying access points (APs) in

This work was supported in part by NSF Award CNS-2209695, by Project RTI2018-102112-B-I00, by ICREA, and by the Fractus Chair on Tech Transfer and 6G.

¹C. Diaz-Vilor and H. Jafarkhani are with the Center for Pervasive Communications and Computing, Univ. of California, Irvine. Emails: {cdiazvil, hamidj} at uci.edu

²A. Lozano is with Universitat Pompeu Fabra (UPF), Barcelona. Email: {angel.lozano} at upf.edu

cellular-based systems, is a research problem of growing interest [2]–[13]. Such flying APs are an attractive alternative to their terrestrial counterparts in terms of coverage, cost, and deployment flexibility. In particular, their flexibility makes flying APs enticing whenever the fixed infrastructure is disrupted. With respect to terrestrial APs, UAVs serving as flying APs pose two distinct challenges: (i) the ground-to-air and air-to-ground character of the radio access links (uplink and downlink, respectively) and (ii) the necessarily wireless nature of the fronthaul connecting the UAVs to the rest of the network. The bulk of the research on this topic has thus far been on the former challenge, including UAV deployment, trajectory optimization, power control, or interference management [14]–[21], always assuming an ideal fronthaul.

Concurrently with the integration of UAVs, wireless systems are progressing towards software-defined architectures [22]–[24] under the umbrella of centralized radio access networks (C-RANs). This goes hand in hand with transcending the time-honored cellular paradigm and moving to cell-free network structures. In such networks, each user can potentially communicate with multiple APs by joint processing of the signals at the APs [25]–[39]. A cell-free framework is especially suitable for UAV networks since UAVs can create strong interference to adjacent cells because of the line-of-sight (LoS) nature of their channels. In a cell-free network, not only can this potential interference be mitigated, but it can actually be turned into useful signals. Initial results confirm the efficacy and benefits of organizing networks where UAVs serve as APs in a cell-free fashion [40], [41]. Again, these early results focus on the radio access, under the premise of ideal fronthauling.

The present paper broadens the scope to encompass both the radio access and the wireless fronthaul, in recognition that an isolated study of one aspect may be deceiving because of potential bottlenecks in the other. With this broader view, UAVs go from being ideal conduits to having to face a constrained wireless fronthaul. This, in turn, brings to the fore issues such as the multiple access in that fronthaul, with alternatives that range from simple frequency-division multiple access (FDMA) to more sophisticated space-division multiple access (SDMA). While this work remains application-agnostic, the performance of the different fronthaul alternatives, and combinations thereof, are tackled. Particularly, the simplicity of FDMA, where the signal isolation reduces the interference, comes at the expense of a higher demand for bandwidth and therefore a reduction in the spectral efficiency. Alternatively, in SDMA, co-channel interference is the price of a multiplexing gain that enables parallelizing transmissions, thereby increasing the spectral efficiency. Finally, the hybrid FDMA-SDMA fronthaul alternative provides more

flexibility and can combine the best of both methods. For the sake of specificity, the paper concentrates on the radio access uplink, with the equally important downlink relegated to future work.

While, motivated by massive MIMO principles, much of the cell-free literature considers matched-filter reception for the radio access uplink [26]–[28], the present work posits minimum mean-square error (MMSE) reception [28]–[30], which is optimum from a signal-to-interference-and-noise (SINR) perspective and reverts to matched filtering in some limiting regimes. This endows the results with broader generality.

With MMSE reception on the radio access and various alternatives for the wireless fronthaul, the analysis then takes place in the asymptotic regime in which the number of UAVs, users, and antennas at the C-RAN gateway, all grow large. This enables leveraging random matrix theory results [42]–[46] to derive deterministic equivalents (finite-dimensional approximations that become exact asymptotically) to the spectral efficiency; importantly, the analysis allows to flexibly define finite subsets of users being served by each UAV, and vice versa, whereby the signal processing complexity remains bounded even as the aforementioned quantities are scaled up. While the aforementioned references study the large-dimensional regime of one-hop cellular networks, to the best of our knowledge this is the first UAV work that provides an asymptotic analysis for two-hop networks, either cellular or cell-free. Two-hop channels are much more difficult to deal with as their overall distribution may not have a closed-form, and in fact the information-theoretic capacity of a multi-hop channel is not yet known. Algorithms that handle point-to-point two-hop settings have been proposed [47]; however, there are still many open problems in a multi-hop network setup. The addition of a wireless fronthaul therefore poses new challenges to UAV networks, especially under Rician fading, where new asymptotic results under zero-forcing reception are derived that might be of independent interest.

Armed with the deterministic equivalents for the spectral efficiency, three key problems are addressed, namely the optimization of (i) the UAV deployment, including altitude, (ii) the user transmit powers, and (iii) the UAV transmit powers. These problems are studied separately given their lack of convexity and, for the deployment problem specifically, a combination of gradient-based (GB) and Gibbs sampling (GS) methods is invoked [48]. The joint optimization of the UAV deployment and the user and UAV transmit powers drastically improves the spectral efficiency, with the lion's share of the benefits being associated with the deployment given that larger feasible sets, i.e., the 3D space, can be explored compared to traditional performance

optimization schemes, such as power or rate control. Altogether, the main contributions of the paper can be summarized as follows:

- An analytical framework is set forth for the uplink of a cell-free UAV network with Rician fading, channel estimation, realistic antenna patterns, and MMSE reception on the radio access, as well as a wireless fronthaul.
- Deterministic equivalents are derived for the spectral efficiency in the above framework, under various fronthaul alternatives.
- For each of the fronthaul alternatives, and with the maximization of the minimum spectral
 efficiency as objective, the UAV deployment and the user and UAV transmit power problems
 are confronted.
- The impact on the optimization gains of network parameters such as the pathloss exponent or the antenna directivity is established.

The remainder of the paper is organized as follows. Sec. II lays down the system and communication models. In Sec. III, the transmission schemes are unveiled, including the cell-free aspects and the different fronthaul alternatives. Then, in Secs. IV–VI, these alternatives are successively studied. Sec. VII subsequently focuses on the deployment optimization problem while numerical results are presented and discussed in Sec. VIII. Concluding remarks are provided in Sec. IX.

II. SYSTEM MODEL

Consider the uplink of a cell-free network featuring M UAVs, located at $\mathbf{q}_m = (x_m, y_m)$ and altitude H_m , serving K cochannel single-antenna users at $\mathbf{w}_k = (\mathbf{x}_k, \mathbf{y}_k)$. The channel coefficient between user k and the single-antenna UAV m is denoted by $g_{k,m}$, drawn from a Rician distribution such that [49, Sec. 3.4.1]

$$g_{k,m} = \sqrt{\frac{\beta_0 g_m(d_{k,m})}{d_{k,m}^{\kappa}}} \left[\sqrt{\frac{K_{k,m}}{K_{k,m}+1}} e^{j\psi_{k,m}} + \sqrt{\frac{1}{K_{k,m}+1}} a_{k,m} \right], \tag{1}$$

where β_0 and κ are the pathloss at a reference distance of 1 m and the pathloss exponent, respectively, while $d_{k,m}$ is the distance. The Rician factor is $K_{k,m} = A_1 e^{A_2 \arcsin(\frac{H_m}{d_{k,m}})}$ for environment-dependent parameters A_1 and A_2 [50]. The phase of the LoS component, $\psi_{k,m}$,

is uniformly random to reflect drifting [34]–[36] whereas $a_{k,m} \sim \mathcal{N}_{\mathbb{C}}(0,1)$ to account for the small-scale fading. Finally, [51]

$$g_m(d_{k,m}) = 2\left(\alpha_m + 1\right) \frac{H_m^{\alpha_m}}{d_{k,m}^{\alpha_m}} \tag{2}$$

models the antenna gain at the mth UAV, with α_m regulating the trade-off between coverage and directivity. Hence, the channel correlation coefficient is

$$r_{k,m} = \mathbb{E}\{|g_{k,m}|^2\}\tag{3}$$

$$= 2\left(\alpha_m + 1\right)\beta_0 \frac{H_m^{\alpha_m}}{d_{k,m}^{\alpha_m + \kappa}}.\tag{4}$$

Upon reception by the UAVs, the collected data is forwarded to the C-RAN gateway, whose coordinates are q=(x,y) with altitude H. Given its air-to-ground nature, a Rician model is invoked for the fronthaul as well. The channel vector connecting the mth UAV with the N-antenna C-RAN gateway is

$$\boldsymbol{h}_{m} = \sqrt{\frac{\beta_{0}}{d_{m}^{\kappa}}} \left[\sqrt{\frac{K_{m}}{K_{m}+1}} e^{j\psi_{m}} \boldsymbol{s}_{m} + \sqrt{\frac{1}{K_{m}+1}} \boldsymbol{a}_{m} \right]$$
 (5)

where d_m and K_m are the distance and Rician factor between UAV m and the C-RAN, respectively. Additionally, ψ_m accounts for the drifting, again modelled as uniformly random. Moreover, $s_m \in \mathbb{C}^{N \times 1}$ is the array response to the mth UAV. For an N-antenna uniform linear array (ULA), the array response satisfies

$$[\mathbf{s}_m]_n = e^{j\frac{2\pi f_c}{c}d(n-1)\sin(\theta_m)\cos(\phi_m)} \tag{6}$$

given the azimuth θ_m , elevation ϕ_m , and antenna spacing d. The small scale fading is $a_m \sim \mathcal{N}_{\mathbb{C}}(0,\Omega_m)$ for some spatial correlation matrix Ω_m among the gateway antennas. Therefore, the overall covariance matrix for a given fronthaul link is

$$\boldsymbol{R}_{m} = \mathbb{E}\{\boldsymbol{h}_{m}\boldsymbol{h}_{m}^{*}\}\tag{7}$$

$$= \frac{\beta_0}{(K_m + 1)d_m^{\kappa}} \left[K_m \boldsymbol{s}_m \boldsymbol{s}_m^* + \boldsymbol{\Omega}_m \right]. \tag{8}$$

A toy example of this two-hop structure containing wireless access and fronthaul is depicted in Fig. 1. While the access links are cell-free-based, the fronthaul allows for FDMA, SDMA or the combination FDMA-SDMA.

¹If multiantenna UAVs were considered, the generalization would be straightforward for IID fading while a spatial correlation matrix would have to be incorporated otherwise.

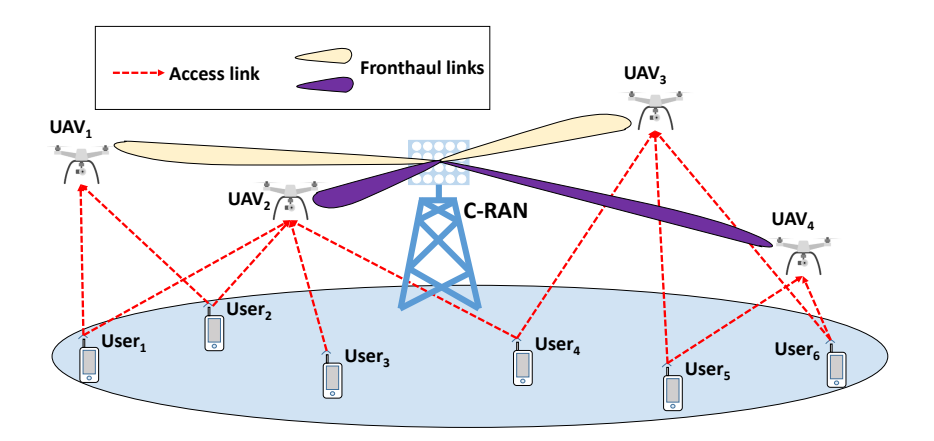


Fig. 1: Cell-free UAV network with wireless access and fronthaul links. In this example, the multiple access employed in the fronthaul is FDMA-SDMA (see Sec. VI).

A. Channel Acquisition

The number of orthogonal pilot dimensions, denoted by τ , is constrained by the coherence bandwidth $B_{\rm c}$ and the coherence time $T_{\rm c}$. The latter depends on the maximum UAV velocity, $v_{\rm max}$, and the carrier frequency, $f_{\rm c}$, with the worst-case dependence being $T_{\rm c} = \frac{c/f_{\rm c}}{2v_{\rm max}}$ for isotropic scattering [49, Sec. 3.4]. The number of resource units within a fading block is $\tau_{\rm c} \approx T_{\rm c} B_{\rm c}$, typically a large number that enables τ to be itself large enough for pilot contamination to be negligible [33], [52]; it also allows for the use of techniques such as random pilots [53]. For instance, at $f_{\rm c} = 2.4$ GHz, and with conservative values $v_{\rm max} = 10$ m/s and $B_{\rm c} = 1$ MHz, we have $\tau_{\rm c} = 6250$. Upon observation of the pilot transmitted by user k at the mth UAV, the MMSE channel estimate $\hat{g}_{k,m}$ satisfies $g_{k,m} = \hat{g}_{k,m} + \tilde{g}_{k,m}$, where $\hat{g}_{k,m}$ is zero-mean with [54]

$$\gamma_{k,m} = \mathbb{E}\{|\hat{g}_{k,m}|^2\} \tag{9}$$

$$=\frac{r_{k,m}^2}{r_{k,m} + \frac{\sigma^2}{p^!\tau}},$$
 (10)

for given τ and p^t , the latter denoting the pilot transmit power, while σ^2 is the noise power at the receiver. In addition, $\tilde{g}_{k,m}$ is zero-mean with variance $c_{k,m} = r_{k,m} - \gamma_{k,m}$. A similar approach is applied to the fronthaul, operating at a frequency different from those of the access links, such that pilot contamination between the two stages is avoided. Concretely, the channel estimates between the mth UAV and the C-RAN gateway satisfy $h_m = \hat{h}_m + \tilde{h}_m$ where \hat{h}_m is zero-mean

with covariance

$$\mathbf{\Phi}_m = \mathbb{E}\{\hat{\mathbf{h}}_m \hat{\mathbf{h}}_m^*\} \tag{11}$$

$$= \mathbf{R}_m \mathbf{\Psi}_m^{-1} \mathbf{R}_m, \tag{12}$$

for $\Psi_m=m{R}_m+rac{\sigma^2}{p^t au}m{I}$. The error, $ilde{m{h}}_m$, is zero-mean with covariance $m{C}_m=m{R}_m-m{\Phi}_m$.

III. DATA TRANSMISSION SCHEMES

This section describes the two-stage data transmission, namely the cell-free radio access and the wireless fronthaul. For the latter, several alternatives are entertained: FDMA, SDMA, and combinations thereof.

A. Cell-Free Radio Access

On a given time-frequency resource unit, the uplink channel matrix is

$$G = (g_1, \dots, g_K), \tag{13}$$

where $\boldsymbol{g}_k \in \mathbb{C}^{M \times 1}$ is the channel between user k and all UAVs, satisfying $\boldsymbol{G} = \hat{\boldsymbol{G}} + \tilde{\boldsymbol{G}}$, with $\hat{\boldsymbol{G}}$ and $\tilde{\boldsymbol{G}}$ being the channel estimation and error matrices, respectively. The subset of UAVs participating in the reception of each user is determined by the binary matrix $\boldsymbol{M}^{(s)} = (\boldsymbol{m}_1^{(s)}, \dots, \boldsymbol{m}_K^{(s)}) \in \mathbb{Z}_2^{M \times K}$ with entries

$$\left[\boldsymbol{M}^{(s)}\right]_{m,k} = \begin{cases} 1 & \text{if } k \in \mathcal{U}_m \\ 0 & \text{otherwise} \end{cases},$$

where \mathcal{U}_m is the set of users regarded as signal by the mth UAV. Its complementary matrix is $M^{(i)} = 1 - M^{(s)}$, with nonzero entries indicating the users that each UAV regards as noise. Pooling the observations from the M UAVs,

$$y = M^{(s)} \circ Gx + M^{(i)} \circ Gx + n \tag{14}$$

$$= M^{(s)} \circ \hat{G}x + (M^{(s)} \circ \tilde{G} + M^{(i)} \circ G)x + n, \tag{15}$$

where \circ denotes Hadamard product, $\boldsymbol{y}=(y_1,\ldots,y_M)^{\mathrm{T}}, \ \boldsymbol{x}=(\sqrt{p_1}s_1,\ldots,\sqrt{p_K}s_K)^{\mathrm{T}}$ with symbols s_k having unit power, p_k being the transmit power, and $\boldsymbol{n}\sim\mathcal{N}_{\mathbb{C}}(\boldsymbol{0},\sigma^2\boldsymbol{I})$.

B. Wireless Fronthaul

At the fronthaul stage, the mth UAV transmits $t_m = \sqrt{\rho_m} y_m$, where

$$\rho_m = \frac{\mathbf{p}_m}{\mathbb{E}\{|y_m|^2\}} \tag{16}$$

$$= \frac{p_m}{\sum_{k=1}^{K} r_{k,m} p_k + \sigma^2}$$
 (17)

ensures an average transmit power of p_m . Within this general framework, the various fronthaul alternatives can be modeled.

1) FDMA: The bandwidth availability at mmWave and sub-THz frequencies makes FDMA an enticing solution, in which signals are perfectly isolated. Here, single-antenna reception at the C-RAN gateway suffices—this is a special case of the FDMA-SDMA strategy with N=1 receive antennas presented later in this section. As a consequence, the observed signal at the C-RAN gateway over the band allocated to the mth UAV is then

$$z_m = h_m t_m + n_m, (18)$$

where $n_m \sim \mathcal{N}_{\mathbb{C}}(0, \sigma^2)$.

2) SDMA: Systems suffering from bandwidth limitations for the fronthaul might consider SDMA, where UAVs transmit concurrently. Their signals are untangled at the C-RAN gateway by the fronthaul combiner $u_m \in \mathbb{C}^{N \times 1}$, with $N \geq M$. At that combiner's output, the signal corresponding to the mth UAV is

$$z_m = \boldsymbol{u}_m^* \bigg(\sum_{j=1}^M \boldsymbol{h}_j t_j + \boldsymbol{n} \bigg), \tag{19}$$

with $n \sim \mathcal{N}_{\mathbb{C}}(\mathbf{0}, \sigma^2 \mathbf{I})$. The structure of \mathbf{u}_m is discussed in the next section.

3) FDMA-SDMA: FDMA and SDMA can be combined. Let the system have $1 \leq L \leq M$ frequency bands, with L=M being FDMA and L=1 being pure SDMA. Over band f_ℓ , a subset of UAVs, denoted by \mathcal{M}_ℓ , conveys data to the C-RAN, which separates the $|\mathcal{M}_\ell|$ streams through an N-dimensional fronthaul combiner, $\boldsymbol{u}_m \in \mathbb{C}^{N \times 1}$. For L>1, the observed signal for $m \in \mathcal{M}_\ell$ is

$$z_m = \boldsymbol{u}_m^* \bigg(\sum_{j \in \mathcal{M}_\ell} \boldsymbol{h}_j t_j + \boldsymbol{n} \bigg), \tag{20}$$

whose terms respectively correspond to the signals from the $|\mathcal{M}_{\ell}|$ UAVs sharing the ℓ th bands and noise.

IV. FDMA FRONTHAUL

Let us now proceed to analyze the performance under FDMA fronthauling. After collecting the M fronthaul transmissions over different bands, the C-RAN receives

$$z = c \circ M^{(s)} \circ \hat{G}x + n'. \tag{21}$$

With the C-RAN treating the fronthaul channel estimate as the true channel, the effective fronthaul gain for the mth UAV is $c_m = \hat{h}_m \sqrt{\rho_m}$; the gains for the M UAVs are assembled into $c = (c_1, \ldots, c_M)$. In turn, n' is the effective noise, zero-mean and with covariance $\Sigma = \mathbb{E}\{n'n'^*\}$. It can be verified that Σ is diagonal, with entries

$$[\mathbf{\Sigma}]_{m,m} = r_m \rho_m \left(\sum_{\forall i} r_{i,m} p_i + \sigma^2 \right) - \phi_m \rho_m \sum_{i \in \mathcal{U}_m} \gamma_{i,m} p_i + \sigma^2.$$
 (22)

Let $\mathcal{F}_k = \{m : [\mathbf{M}^{(s)}]_{m,k} = 1, m = 1, \dots, M\}$ be the subset of UAVs that regard what is received from user k as signal. From the rows of z whose indices are in \mathcal{F}_k , we obtain the $|\mathcal{F}_k| \times 1$ vector

$$\boldsymbol{z}_k = \boldsymbol{c}_k \circ \boldsymbol{M}_k^{(s)} \circ \hat{\boldsymbol{G}}_k \boldsymbol{x} + \boldsymbol{n}_k', \tag{23}$$

where $\boldsymbol{M}_{k}^{(s)}=(\boldsymbol{m}_{k,1}^{(s)},\ldots,\boldsymbol{m}_{k,K}^{(s)})\in\mathbb{Z}_{2}^{|\mathcal{F}_{k}|\times K},\ \boldsymbol{c}_{k}\in\mathbb{C}^{|\mathcal{F}_{k}|\times|\mathcal{F}_{k}|},\ \hat{\boldsymbol{G}}_{k}\in\mathbb{C}^{|\mathcal{F}_{k}|\times K}$ and $\boldsymbol{n}_{k}'\in\mathbb{C}^{|\mathcal{F}_{k}|\times 1}$ contain the \mathcal{F}_{k} rows of the original matrices and vectors. For a generic combiner, $\boldsymbol{w}_{k}\in\mathbb{C}^{|\mathcal{F}_{k}|\times 1}$, the instantaneous SINR experienced by user k is

$$SINR_{k} = \frac{|\boldsymbol{w}_{k}^{*}(\boldsymbol{c}_{k} \circ \hat{\boldsymbol{g}}_{k})|^{2} p_{k}}{\boldsymbol{w}_{k}^{*} \left(\sum_{i \neq k} (\boldsymbol{c}_{k} \circ \boldsymbol{m}_{k,i}^{(s)} \circ \hat{\boldsymbol{g}}_{i}) (\boldsymbol{c}_{k} \circ \boldsymbol{m}_{k,i}^{(s)} \circ \hat{\boldsymbol{g}}_{i})^{*} p_{i} + \boldsymbol{\Sigma}_{k}\right) \boldsymbol{w}_{k}^{*}},$$
(24)

achieving a spectral efficiency of

$$SE_k = \frac{1}{L} \left(1 - \frac{\tau}{\tau_c} \right) \mathbb{E} \{ \log_2 (1 + SINR_k) \}, \tag{25}$$

where $\frac{\tau}{\tau_c}$ accounts for the pilot overhead and L represents the number of fronthaul frequency bands; in this case L=M. Consequently, although an increase in M yields higher SINR values, the pre-log factor dominates (25) and therefore the overall spectral efficiency decreases. With the optimum MMSE combiner, the above specializes to [29]

$$SINR_k = (\boldsymbol{c}_k \circ \hat{\boldsymbol{g}}_k)^* \left(\sum_{i \neq k} (\boldsymbol{c}_k \circ \boldsymbol{m}_{k,i}^{(s)} \circ \hat{\boldsymbol{g}}_i) (\boldsymbol{c}_k \circ \boldsymbol{m}_{k,i}^{(s)} \circ \hat{\boldsymbol{g}}_i)^* p_i + \boldsymbol{\Sigma}_k \right)^{-1} (\boldsymbol{c}_k \circ \hat{\boldsymbol{g}}_k) p_k.$$
(26)

A. Large-Dimensional Analysis

The evaluation of (25) takes place in the asymptotic regime, $|\mathcal{F}_k|, |\mathcal{U}_m| \to \infty \ \forall k, m$, where convergence to nonrandom limits is assured provided that

$$\Gamma_k = \mathbb{E}\Big\{ \big(\boldsymbol{m}_k^{(s)} \circ \hat{\boldsymbol{g}}_k \big) \big(\boldsymbol{m}_k^{(s)} \circ \hat{\boldsymbol{g}}_k \big)^* \Big\}$$
(27)

$$=\operatorname{diag}\{\gamma_{k,m}m_{k,m}^{(s)}\ \forall m\},\tag{28}$$

and

$$\Phi = \mathbb{E}\Big\{\hat{\boldsymbol{h}}\hat{\boldsymbol{h}}^*\Big\} \tag{29}$$

$$= \operatorname{diag}\{\phi_m \,\forall m\},\tag{30}$$

with $\hat{h} = (\hat{h}_1, \dots, \hat{h}_M)^T$ satisfying some technical conditions. Specifically, the inverse of the resolvent matrix in (26) must exist, which is ensured by the presence of Σ_k , while Γ_k and Φ must have uniformly bounded spectral norms. In other words, the received power should not concentrate on a subset of dimensions as the network grows large.

Theorem 1. With an FDMA fronthaul, $|\mathcal{F}_k|, |\mathcal{U}_m| \to \infty \ \forall \ k, m \ and \ MMSE \ subset \ combining, <math>SINR_k - \overline{SINR}_k \stackrel{\text{a.s.}}{\to} 0$ almost surely (a.s.) with $\overline{SINR}_k = \sum_{m \in \mathcal{F}_k} \overline{SINR}_{k,m}$ and

$$\overline{SINR}_{k,m} = \frac{\gamma_{k,m} p_k}{\sum\limits_{\substack{i \in \mathcal{U}_m \\ i \neq k}} \frac{\gamma_{i,m}}{1 + e_i} p_i + \frac{r_m}{\phi_m} \left(\sum\limits_{\forall i} r_{i,m} p_i + \sigma^2\right) - \sum\limits_{\substack{i \in \mathcal{U}_m \\ \gamma_{i,m} p_i + \frac{\sigma^2}{\phi_m \rho_m}}}.$$
 (31)

The coefficients e_j are obtained iteratively by $e_j = \lim_{n \to \infty} e_j^{(n)}$, $e_j^{(0)} = |\mathcal{F}_j|$, and

$$e_j^{(n)} = p_j \operatorname{tr} \left[\mathbf{\Phi} \mathbf{\Gamma}_j \left(\sum_{i \neq j}^K \frac{\mathbf{\Phi} \mathbf{\Gamma}_i}{1 + e_i^{(n-1)}} p_i + \mathbf{\Sigma}_j \right)^{-1} \right].$$
 (32)

Proof. Details on how (31) emanates from [45], [46] can be found in Appendix C. \Box

Interestingly, note that in the asymptotic regime, the value of $\overline{\text{SINR}}_k$ is a linear combination of the SINRs that the kth user experiences over the \mathcal{F}_k UAVs weighted by the fronthaul channel. Finally, from the continuous mapping theorem [55], $\text{SE}_k - \frac{1}{M} \left(1 - \frac{\tau}{\tau_c}\right) \log_2(1 + \overline{\text{SINR}}_k) \stackrel{\text{a.s.}}{\to} 0$.

B. Problem Formulation

Let us now turn to optimizing the UAV deployment and transmit powers. With the aim of ensuring fairness in the network, this is formulated as the max-min problem

$$\max_{\boldsymbol{q}_{m}, H_{m}, p_{k}, \mathbf{p}_{m}} \min_{k} \frac{1}{M} \left(1 - \frac{\tau}{\tau_{c}} \right) \mathbb{E} \{ \log_{2} (1 + \operatorname{SINR}_{k}) \}$$
s.t. $H_{\min} \leq H_{m} \leq H_{\max}, \ p_{k} \leq p_{\max}, \ \mathbf{p}_{m} \leq \mathbf{p}_{\max},$

$$(33)$$

which is nonconvex. Invoking Thm. 1, and with the constraints not reiterated for the sake of compactness, the above leads to

$$\max_{\boldsymbol{q}_m, H_m, p_k, \mathbf{p}_m} \min_{k} \sum_{m \in \mathcal{F}_k} \overline{\text{SINR}}_{k, m}, \tag{34}$$

where $\overline{SINR}_{k,m}$ is provided in (31). The optimizations of UAV deployment and transmit powers are tacked separately as follows.

1) Deployment Optimization: The analytical 2D-gradients w.r.t. (34) for a given altitude are

$$\nabla_{\boldsymbol{q}_j} \overline{\mathrm{SINR}}_k = \frac{\nabla_{\boldsymbol{q}_j} \gamma_{k,j} \, \mathrm{Den}_j - \gamma_{k,j} \nabla_{\boldsymbol{q}_j} \mathrm{Den}_j}{\mathrm{Den}_j^2} p_k \ \text{ for } j \in \mathcal{F}_k,$$
 (35)

where Den_j is the denominator of (31). The optimization of H_m is studied separately, as it is common to every fronthaul alternative.

2) User Transmit Power: The following result is a stepping stone to the user transmit power optimization.

Proposition 1. The objective function $\min_k \overline{SINR}_k$ in (33) satisfies the definition of competitive utility function while the constraints $p_k \leq p_{\max}$ follow the definition of monotonic constraints.

Capitalizing on Prop. 1, the algorithm in [56, Alg. 1] can be applied with sure converge to the optimum user transmit power in the max-min SINR sense.

3) UAV Transmit Power: From (31), it can be shown that $\overline{SINR}_{k,m}$ is an increasing function of p_m . Consequently, \overline{SINR}_k increases with p_m as well. Therefore, the optimal UAV transmit power that maximizes the $\min_k \overline{SINR}_k$ is $p_m = p_{max}$.

V. SDMA FRONTHAUL

Let us now turn to the SDMA fronthaul alternative. The C-RAN received signals still follow (21) after applying the N-dimensional combiner u_m in (19) and replacing $c_m = u_m^* \hat{h}_m \sqrt{\rho_m}$ and the equivalent noise

$$n'_{m} = \sum_{j=1}^{M} \boldsymbol{u}_{m}^{*} \boldsymbol{h}_{j} \sqrt{\rho_{j}} y_{j} - \boldsymbol{u}_{m}^{*} \hat{\boldsymbol{h}}_{m} \sqrt{\rho_{m}} \left(\sum_{k \in \mathcal{U}_{m}} \hat{g}_{k,m} x_{k} \right) + \boldsymbol{u}_{m}^{*} \boldsymbol{n}.$$
(36)

The SINR and spectral efficiency expressions in (25)–(26), corresponding to an MMSE access combiner, also hold with the aforementioned modifications. In particular, the pre-log factor only depends on the pilot overhead when L=1.

A zero-forcing (ZF) structure is adopted for the fronthaul, whereby $U = (u_1, \ldots, u_M) \in \mathbb{C}^{N \times M}$ is given by $U = \hat{H}(\hat{H}^*\hat{H})^{-1}$ with $\hat{H} = (\hat{h}_1, \ldots, \hat{h}_M)$. Then, $u_m^*\hat{h}_j = \delta_{m,j}$ with $\delta_{m,j} = 1$ if m = j and 0 otherwise. The ensuing SINR involves the equivalent noise power $\mathbb{E}\{n_m'n_j'^*\}$ under Rician fading, for which no expressions are available in the literature. One of the contributions in the sequel is an asymptotic expression for this power.

A. Large-Dimensional Analysis

As in Sec. IV-A, the spectral efficiency is evaluated for $|\mathcal{F}_k|$, $|\mathcal{U}_m| \to \infty \ \forall k, m$ and $N \to \infty$ with $N \ge M$. Convergence to deterministic limits is assured provided that \mathbf{R}_m satisfies the same conditions as Φ and Γ_m . As the equivalent noise n'_m in (36) satisfies $\mathbb{E}\{n'_m n'^*_j\} \propto \mathbb{E}\{\mathbf{u}_m^* \mathbf{Q} \mathbf{u}_j\}$, we first proceed to characterize such quadratic form asymptotically with a result that might be of independent interest.

Theorem 2. Let $Q \in \mathbb{C}^{N \times N}$ be a deterministic Hermitian matrix while $U = (u_1, \dots, u_M) \in \mathbb{C}^{N \times M}$ is a ZF matrix combiner, $U = \lim_{\epsilon \to 0} \hat{H} (\hat{H}^* \hat{H} + \epsilon I)^{-1}$. For $M, N \to \infty$,

$$\mathbb{E}\{\boldsymbol{u}_{m}^{*}\boldsymbol{Q}\boldsymbol{u}_{m}\} - \lim_{\epsilon \to 0} \frac{\frac{1}{N^{2}} \operatorname{tr}\left(\boldsymbol{\Phi}_{m} \boldsymbol{T}'(\epsilon, \boldsymbol{Q})\right)}{\left(1 + \frac{1}{N} \operatorname{tr}(\boldsymbol{\Phi}_{m} \boldsymbol{T})\right)^{2}} \stackrel{\text{a.s.}}{\to} 0$$
(37)

for T and $T'(\epsilon, Q)$ defined in (67) and (69), respectively.

The convergence of (37), in terms of relative error, is illustrated in Fig. 2.

Corollary 1. Let $Q \in \mathbb{C}^{N \times N}$ be a deterministic Hermitian matrix while $U = (u_1, \dots, u_M) \in \mathbb{C}^{N \times M}$ is a ZF matrix combiner, $U = \lim_{\epsilon \to 0} \hat{\boldsymbol{H}} (\hat{\boldsymbol{H}}^* \hat{\boldsymbol{H}} + \epsilon \boldsymbol{I})^{-1}$. For $M, N \to \infty$, and $m \neq j$

$$\mathbb{E}\{\boldsymbol{u}_{m}^{*}\boldsymbol{Q}\boldsymbol{u}_{j}\}\stackrel{\text{a.s.}}{\to}0. \tag{38}$$

Proof. The proof follows similar steps as the ones included in Appendix E and exploits the fact that \hat{h}_m and \hat{h}_j are uncorrelated.

The combination of Thm. 2 and Corollary 1 results in an asymptotically diagonal noise covariance matrix Σ_k .

Theorem 3. With an SDMA fronthaul, ZF fronthaul combining, $|\mathcal{F}_k|$, $|\mathcal{U}_m| \to \infty \ \forall \ k, m, \ N \to \infty$ with $N \ge M$ and MMSE subset combining, $SINR_k - \overline{SINR}_k \overset{\text{a.s.}}{\to} 0$ with $\overline{SINR}_k = \sum_{m \in \mathcal{F}_k} \overline{SINR}_{k,m}$ and

$$\overline{SINR}_{k,m} = \frac{\gamma_{k,m} p_k}{\sum\limits_{\substack{i \in \mathcal{U}_m \\ i \neq k}} \frac{\gamma_{i,m}}{1 + e_i} p_i + \sum\limits_{\forall i} r_{i,m} p_i - \sum\limits_{\substack{i \in \mathcal{U}_m \\ i \in \mathcal{U}_m}} \gamma_{i,m} p_i + \sigma^2 + \frac{\xi_m^{SDMA}}{\rho_m}}.$$
 (39)

The application of Thm. 2 to $\mathbb{E}\{n'_m n'^*_m\}$ results in

$$\xi_m^{SDMA} = \lim_{\epsilon \to 0} \sum_{n=1}^M p_n \frac{\frac{1}{N^2} \text{tr}(\boldsymbol{\Phi}_m \boldsymbol{T}'(\epsilon, \boldsymbol{C}_n))}{\left(1 + \frac{1}{N} \text{tr}(\boldsymbol{\Phi}_m \boldsymbol{T})\right)^2} + \sigma^2 \frac{\frac{1}{N^2} \text{tr}(\boldsymbol{\Phi}_m \boldsymbol{T}'(\epsilon, \boldsymbol{I}))}{\left(1 + \frac{1}{N} \text{tr}(\boldsymbol{\Phi}_m \boldsymbol{T})\right)^2}$$
(40)

while the coefficients e_j are obtained iteratively by $e_j = \lim_{n \to \infty} e_j^{(n)}$, $e_j^{(0)} = |\mathcal{F}_j|$, and

$$e_j^{(n)} = \sum_{m \in \mathcal{F}_j} \frac{\gamma_{j,m} p_j}{\sum\limits_{\substack{i \in \mathcal{U}_m \\ i \neq k}} \frac{\gamma_{i,m}}{1 + e_i^{(n-1)}} p_i + \sum\limits_{\forall i} r_{i,m} p_i - \sum\limits_{\substack{i \in \mathcal{U}_m }} \gamma_{i,m} p_i + \sigma^2 + \frac{\xi_m^{SDMA}}{\rho_m}}.$$
(41)

Proof. Proceed as in Appendix C.

Similarly to the FDMA case, $\overline{\mathrm{SINR}}_k$ can be decomposed as the sum of SINRs over the \mathcal{F}_k UAVs with two main differences: (i) the fronthaul channel is compensated by the ZF combiner and (ii) the noise is increased after the ZF stage, as per $\frac{\xi_m^{\mathrm{SDMA}}}{\rho_m}$. Finally, from the continuous mapping theorem, $\mathrm{SE}_k - \left(1 - \frac{\tau}{\tau_c}\right) \log_2(1 + \overline{\mathrm{SINR}}_k) \overset{\mathrm{a.s.}}{\to} 0$.

B. Problem Formulation

We now turn to optimizing the UAV deployment and transmit powers by maximizing the minimum SINR under SDMA fronthauling. Capitalizing on Thm. 3, that amounts to

$$\max_{\boldsymbol{q}_{m}, H_{m}, p_{k}, \mathbf{p}_{m}} \min_{k} \sum_{m \in \mathcal{F}_{k}} \overline{\text{SINR}}_{k, m}$$
s.t. $H_{\min} \leq H_{m} \leq H_{\max}, \ p_{k} \leq p_{\max}, \ \mathbf{p}_{m} \leq \mathbf{p}_{\max},$

$$(42)$$

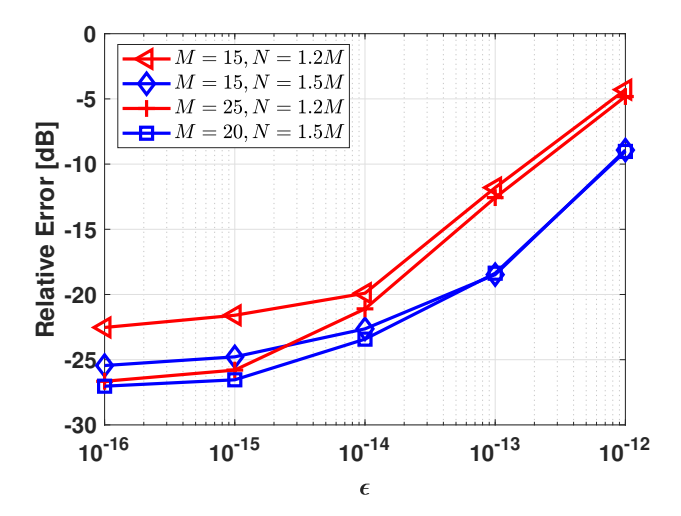


Fig. 2: Relative error between the two terms in Thm. 2 as a function of ϵ for various M and N.

for $\overline{SINR}_{k,m}$ in (39). The above problem is nonconvex.

1) Deployment Optimization: The presence of $\xi_m^{\rm SDMA}$ in the denominator of (39) makes the gradients analytically unwieldy. However, as shown in Fig. 3a, the signal terms within $\xi_m^{\rm SDMA}$ satisfy

$$\lim_{\epsilon \to 0} \frac{\frac{1}{N^2} \operatorname{tr}(\boldsymbol{\Phi}_m \boldsymbol{T}'(\epsilon, \boldsymbol{C}_n))}{\left(1 + \frac{1}{N} \operatorname{tr}(\boldsymbol{\Phi}_m \boldsymbol{T})\right)^2} \approx c_m d_m^{\kappa},\tag{43}$$

where c_m is a regression parameter and d_m , recall, is the distance between UAV m and the C-RAN. Referring to Fig. 3a, c_m can be obtained by fitting every data point (solid regression curve) or only the maximum at each distance (dashed regression curve). Similarly for the noise term within $\xi_m^{\rm SDMA}$, as shown in Fig. 3b,

$$\lim_{\epsilon \to 0} \frac{\frac{1}{N^2} \operatorname{tr}(\boldsymbol{\Phi}_m \boldsymbol{T}'(\epsilon, \boldsymbol{I}))}{\left(1 + \frac{1}{N} \operatorname{tr}(\boldsymbol{\Phi}_m \boldsymbol{I})\right)^2} \approx c_m^{(n)} d_m^{\kappa}, \tag{44}$$

with a corresponding regression parameter $c_m^{(n)}$. After comparing the respective performances, the solid regression curves are chosen and the gradient satisfies

$$\nabla_{\boldsymbol{q}_m} \overline{\mathrm{SINR}}_k \approx \frac{\nabla_{\boldsymbol{q}_m} \gamma_{k,m} \, \mathrm{Den}_m - \gamma_{k,m} \nabla_{\boldsymbol{q}_m} \mathrm{Den}_m}{\mathrm{Den}_m^2} p_k \ \text{ for } m \in \mathcal{F}_k., \tag{45}$$

with

$$Den_m = \sum_{\substack{i \in \mathcal{U}_m \\ i \neq k}} \frac{\gamma_{i,m}}{1 + e_i} p_i + \sum_{\forall i} r_{i,m} p_i - \sum_{i \in \mathcal{U}_m} \gamma_{i,m} p_i + \sigma^2 + \frac{d_m^{\kappa}}{\rho_m} \left(\sum_{n=1}^M p_n c_m + \sigma^2 c_m^{(n)} \right).$$
(46)

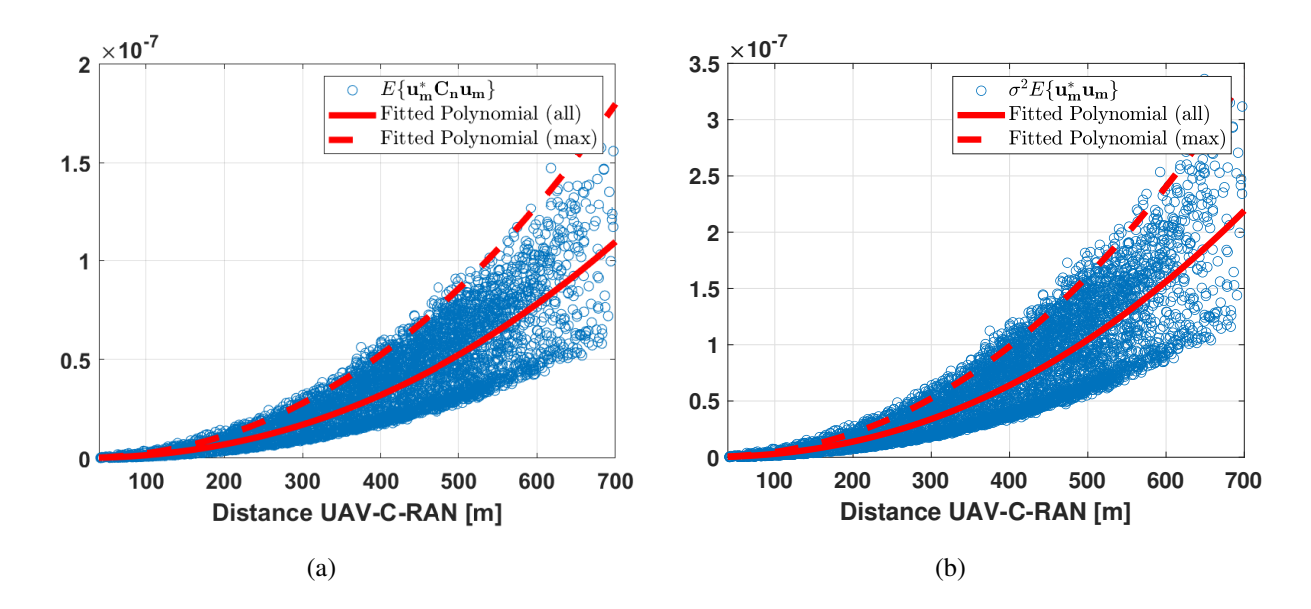


Fig. 3: Curve fitting with every data point (solid) or only the maximum at each distance (dashed) for (a) $\mathbb{E}\{u_m^*C_nu_m\}$ and (b) $\sigma^2\mathbb{E}\{u_m^*u_m\}$.

- 2) User Transmit Power: It can be verified that $\min_k \overline{SINR}_k$ in (42) satisfies the definition of competitive utility function and the constraints are monotonic. Thus, [56, Alg. 1] converges to the optimal user transmit powers.
- 3) UAV Transmit Power: To tackle this subproblem, it is convenient to reformulate (42) so as to capitalize on the fact that for any set of functions $f_k(x)$, the problem $\max_x \min_k f_k(x)$ is equivalent to

$$\max_{\boldsymbol{x},t} t$$

$$\text{s.t.} f_k(\boldsymbol{x}) \ge t \ \forall k.$$
(47)

It follows that the optimization in (42) w.r.t. p_m is equivalent to

$$\max_{\mathbf{p}_{m}, t, y_{k,m}} t$$
s.t.
$$\sum_{m \in \mathcal{F}_{k}} y_{k,m}^{2} \ge t \ \forall k$$

$$y_{k,m}^{2} \le \overline{\text{SINR}}_{k,m} \ \forall k, m$$

$$(48)$$

where $y_{k,m}$ is a slack variable satisfying $y_{k,m}^2 = \overline{\text{SINR}}_{k,m}$ when the optimum solution is attained; elsewhere, the value of $y_{k,m}^2$ can be increased for a higher cost function.

While equivalent to the original problem, (48) is neither convex nor concave. To tackle it, we leverage the successive convex approximation method (SCA) [57]. First, given that $y_{k,m}^2$ is convex, it accepts a lower bound of the type $y_{k,m}^2 \ge y_{k,m}^{2 \text{ (lb)}}$ with

$$y_{k,m}^{2 \text{ (lb)}} = y_{k,m}^{2 \text{ (p)}} + 2y_{k,m}^{(p)}(y_{k,m} - y_{k,m}^{(p)})$$

$$\tag{49}$$

where $y_{k,m}^{2 \text{ (p)}}$ is the value of $y_{k,m}^2$ at approximation point p. Then, defining for the sake of brevity

$$\lambda_{m,n} = \lim_{\epsilon \to 0} \frac{\frac{1}{N^2} \operatorname{tr}(\boldsymbol{\Phi}_m \boldsymbol{T}'(\epsilon, \boldsymbol{C}_n))}{\left(1 + \frac{1}{N} \operatorname{tr}(\boldsymbol{\Phi}_m \boldsymbol{T})\right)^2}$$
 (50)

and

$$\lambda_{m}' = \lim_{\epsilon \to 0} \frac{\frac{1}{N^{2}} \operatorname{tr}(\boldsymbol{\Phi}_{m} \boldsymbol{T}'(\epsilon, \boldsymbol{I}))}{\left(1 + \frac{1}{N} \operatorname{tr}(\boldsymbol{\Phi}_{m} \boldsymbol{I})\right)^{2}},\tag{51}$$

a similar procedure is followed to derive a lower bound for $\overline{\text{SINR}}_{k,m}$, which is convex w.r.t. $\frac{1}{p_m} \left(\sum_{n \neq m}^M \lambda_{m,n} r_n p_n + \sigma^2 \lambda_m' \right)$ and therefore satisfies $\overline{\text{SINR}}_{k,m} \geq \overline{\text{SINR}}_{k,m}^{(\text{lb})}$ with

$$\overline{\text{SINR}}_{k,m}^{(\text{lb})} = \overline{\text{SINR}}_{k,m}^{(\text{p})} - \zeta_{k,m}^{\text{SD}} \left[\frac{1}{p_m} \left(\sum_{n=1}^{M} \lambda_{m,n} r_n p_n + \sigma^2 \lambda_m' \right) - \frac{1}{p_m^{(\text{p})}} \left(\sum_{n=1}^{M} \lambda_{m,n} r_n p_n^{(\text{p})} + \sigma^2 \lambda_m' \right) \right]$$
(52)

and with

$$\zeta_{k,m}^{\text{SD}} = -\frac{\partial \overline{\text{SINR}}_{k,m}}{\partial \frac{1}{p_m} \left(\sum_{n=1}^M \lambda_{m,n} r_n p_n + \sigma^2 \lambda_m' \right)} \bigg|_{p_i = p_i^{(p)} \ i = 1, \dots, M}.$$
(53)

Still, $y_{k,m}^2 \leq \overline{\text{SINR}}_{k,m}^{(\text{lb})}$ is not convex because of the quotients $\frac{\mathbf{p}_n}{\mathbf{p}_m}$ in (52). Division of both sides of the inequality by $\sum_{n=1}^{M} \lambda_{m,n} r_n \mathbf{p}_n + \sigma^2 \lambda_m'$ gives

$$\frac{y_{k,m}^{2}}{\sum_{n=1}^{M} \lambda_{m,n} r_{n} \mathbf{p}_{n} + \sigma^{2} \lambda'_{m}} \leq -\frac{\zeta_{k,m}^{\text{SD}}}{\mathbf{p}_{m}} + \frac{\overline{\text{SINR}}_{k,m}^{(p)} + \frac{\zeta_{k,m}^{\text{SD}}}{p_{m}^{(p)}} \left(\sum_{n=1}^{M} \lambda_{m,n} r_{n} \mathbf{p}_{n}^{(p)} + \sigma^{2} \lambda'_{m}\right)}{\sum_{n=1}^{M} \lambda_{m,n} r_{n} \mathbf{p}_{n} + \sigma^{2} \lambda'_{m}},$$
(54)

where the only nonconvex term is the second in the right-hand side, which itself accepts a lower bound w.r.t. $\sum_{n=1}^{M} \lambda_{m,n} r_n p_n + \sigma^2$. As a consequence, further application of the SCA technique results in the convex set of constraints

$$\frac{y_{k,m}^{2}}{\sum_{n=1}^{M} \lambda_{m,n} r_{n} p_{n} + \sigma^{2} \lambda_{m}'} \leq -\frac{\zeta_{k,m}^{SD}}{p_{m}} + \left[\overline{SINR}_{k,m} + \frac{\zeta_{k,m}^{SD}}{p_{m}^{(p)}} \left(\sum_{n=1}^{M} \lambda_{m,n} r_{n} p_{n}^{(p)} + \sigma^{2} \lambda_{m}' \right) \right] \times \left[\frac{1}{\sum_{n=1}^{M} \lambda_{m,n} r_{n} p_{n}^{(p)} + \sigma^{2} \lambda_{m}'} - \frac{1}{\left(\sum_{n=1}^{M} \lambda_{m,n} r_{n} p_{n}^{(p)} + \sigma^{2} \lambda_{m}' \right)^{2}} \left(\sum_{n=1}^{M} \lambda_{m,n} r_{n} p_{n}^{(p)} - \sum_{n=1}^{M} \lambda_{m,n} r_{n} p_{n}^{(p)} \right) \right].$$
(55)

Altogether then, an approximate convex reformulation of (48) is

$$\max_{\mathbf{p}_{m}, t, y_{k,m}} t$$
s.t.
$$\sum_{m \in \mathcal{F}_{k}} y_{k,m}^{2 \text{ (lb)}} \ge t \ \forall k$$
(56)

and further subject to (55). This problem can be efficiently solved with standard optimization tools [58]. In addition, it can be shown that, given the tightness of the local approximations, the sequence of objective values generated by the SCA applied to (56) is monotonically non-decreasing with an upper bound, and therefore converges.

VI. FDMA-SDMA

Finally, under a combined FDMA and SDMA fronthaul, the application of the N-dimensional fronthaul combiner \boldsymbol{u}_m in (20) yields the same model of (21) with $c_m = \boldsymbol{u}_m^* \hat{\boldsymbol{h}}_m \sqrt{\rho_m}$ and an equivalent noise $\boldsymbol{n}' = (n'_1, \dots, n'_M) \in \mathbb{C}^{M \times 1}$ with

$$n'_{m} = \sum_{j \in \mathcal{M}_{\ell}}^{M} \boldsymbol{u}_{m}^{*} \boldsymbol{h}_{j} \sqrt{\rho_{j}} y_{j} - \boldsymbol{u}_{m}^{*} \hat{\boldsymbol{h}}_{m} \sqrt{\rho_{m}} \left(\sum_{k \in \mathcal{U}_{m}} \hat{g}_{k,m} x_{k} \right) + \boldsymbol{u}_{m}^{*} \boldsymbol{n}_{c}.$$
 (57)

The SDMA component requires $N \geq \max\{|\mathcal{M}_{\ell}|, \ell = 1, ..., L\}$ and, with the fronthaul combiner \boldsymbol{u}_m set to be ZF, $\boldsymbol{u}_m^* \hat{\boldsymbol{h}}_j = \delta_{m,j}$ for $m, j \in \mathcal{M}_{\ell}$.

A. Large-Dimensional Analysis

Under the same assumptions as for pure FDMA or SDMA and given the ZF nature of u_m , Thm. 2 is applied to characterize the asymptotic equivalent noise terms.

Theorem 4. With a combined FDMA and ZF-SDMA fronthaul, $|\mathcal{F}_k|$, $|\mathcal{U}_m| \to \infty \ \forall \ k, m, \ N \to \infty$ with $N \ge \max\{|\mathcal{M}_\ell|, \ \ell = 1, \dots, L\}$, and MMSE subset combining, $SINR_k - \overline{SINR}_k \overset{a.s.}{\to} 0$ with $\overline{SINR}_k = \sum_{m \in \mathcal{F}_k} \overline{SINR}_{k,m}$ and

$$\overline{SINR}_{k,m} = \frac{\gamma_{k,m} p_k}{\sum\limits_{\substack{i \in \mathcal{U}_m \\ i \neq k}} \frac{\gamma_{i,m}}{1 + e_{i,k}} p_i + \sum\limits_{\forall i} r_{i,m} p_i - \sum\limits_{\substack{i \in \mathcal{U}_m \\ i \in \mathcal{U}_m}} \gamma_{i,m} p_i + \sigma^2 + \frac{\xi_m^{FS}}{\rho_m}}.$$
 (58)

The application of Thm. 2 to $\mathbb{E}\{n'_m n'^*_m\}$ results in

$$\xi_m^{FS} = \lim_{\epsilon \to 0} \sum_{j \in \mathcal{M}_{\ell}} p_j \frac{\frac{1}{N^2} \text{tr}(\boldsymbol{\Phi}_m \boldsymbol{T}'(\epsilon, \boldsymbol{C}_j))}{\left(1 + \frac{1}{N} \text{tr}(\boldsymbol{\Phi}_m \boldsymbol{T})\right)^2} + \sigma^2 \frac{\frac{1}{N^2} \text{tr}(\boldsymbol{\Phi}_m \boldsymbol{T}'(\epsilon, \boldsymbol{I}))}{\left(1 + \frac{1}{N} \text{tr}(\boldsymbol{\Phi}_m \boldsymbol{I})\right)^2}.$$
 (59)

The coefficients e_j are obtained iteratively by $e_j = \lim_{n \to \infty} e_j^{(n)}$, $e_j^{(0)} = |\mathcal{F}_j|$, and

$$e_{j}^{(n)} = \sum_{m \in \mathcal{F}_{j}} \frac{\gamma_{i,m}}{\sum_{\substack{i \in \mathcal{U}_{m} \\ i \neq j}} \frac{\gamma_{i,m}}{1 + e_{i}^{(n-1)}} p_{i} + \sum_{\forall i} r_{i,m} p_{i} - \sum_{\substack{i \in \mathcal{U}_{m} \\ i \in \mathcal{U}_{m}}} \gamma_{i,m} p_{i} + \sigma^{2} + \frac{\xi_{m}^{FS}}{\rho_{m}}.$$
 (60)

Proof. Proceed as in Appendix C.

From the continuous mapping theorem, $SE_k - \frac{1}{L} \left(1 - \frac{\tau}{\tau_c} \right) \log_2(1 + \overline{SINR}_k) \stackrel{\text{a.s.}}{\to} 0.$

B. Problem Formulation

The max-min SINR optimization problem in this case boils down to

$$\max_{\boldsymbol{q}_{m}, H_{m}, p_{k}, p_{m}} \min_{k} \sum_{m \in \mathcal{F}_{k}} \overline{\text{SINR}}_{k, m}$$
s.t. $H_{\min} \leq H_{m} \leq H_{\max}, \ p_{k} \leq p_{\max}, \ p_{m} \leq p_{\max},$

$$(61)$$

for $\overline{SINR}_{k,m}$ given in (58).

1) Deployment Optimization: As in pure SDMA, the terms in ξ_m^{FS} can be approximated by a linear combination of polynomials whose variable is the distance between the UAV and the C-RAN. Therefore,

$$\nabla_{\boldsymbol{q}_m} \overline{\mathrm{SINR}}_k \approx \frac{\nabla_{\boldsymbol{q}_m} \gamma_{k,m} \, \mathrm{Den}_m - \gamma_{k,m} \nabla_{\boldsymbol{q}_m} \mathrm{Den}_m}{\mathrm{Den}_m^2} p_k \text{ for } m \in \mathcal{F}_k, \tag{62}$$

where

$$Den_m = \sum_{\substack{i \in \mathcal{U}_m \\ i \neq k}} \frac{\gamma_{i,m}}{1 + e_{i,k}} p_i + \sum_{\forall i} r_{i,m} p_i - \sum_{i \in \mathcal{U}_m} \gamma_{i,m} p_i + \sigma^2 + \frac{d_m^{\kappa}}{\rho_m} \left(\sum_{j \in \mathcal{M}_{\ell}} p_j c_m + \sigma^2 c_m^{(n)} \right).$$
(63)

- 2) User Power Allocation: Again, [56, Alg. 1] converges to the user transmit power that maximizes $\min_k \overline{SINR}_k$ in (61).
- 3) UAV Power Allocation: Because of space limitations, the derivation of the UAV transmit power optimization is not included. Similar steps as in Sec. IV-B3 should be followed.

VII. GB-GS DEPLOYMENT ALGORITHM

Equipped with the 2D gradients derived in the previous section, the UAV locations could be updated iteratively as

$$\boldsymbol{q}_{m}^{(t)} \leftarrow \boldsymbol{q}_{m}^{(t)} + \rho^{(t)} \nabla_{\boldsymbol{q}_{m}} \overline{\text{SINR}}_{k}^{(t)}|_{\boldsymbol{q}_{m} = \boldsymbol{q}_{m}^{(t)}}, \tag{64}$$

where t is the iteration counter and $\rho^{(t)}$ a decreasing function of t for convergence reasons. However, the nonconvex nature of the problem may result in low-quality solutions. Moreover, the altitudes should be part of the optimization as well. For such a complex optimization, an attractive approach is that of stochastic optimization. This work leverages the well-known GS technique in conjunction with (64). Concretely, for a set of possible states Θ , GS aims at solving

$$\max_{\{\ell_m \,\forall m\} \in \Theta} \, \min_k \, \overline{\text{SINR}}_k, \tag{65}$$

where $\ell_m = (q_m, H_m)$ corresponds to the 3D locations that are iteratively updated according to a certain probability distribution [48].

Let $\eta^{(t)} = \min_k \overline{\mathrm{SINR}}_k^{(t)} \equiv \overline{\mathrm{SINR}}_{k_{\min}^{(t)}}^{(t)}$ be the cost function at Iteration t whereas $k_{\min}^{(t)}$ represents the index of the user with lowest $\overline{\mathrm{SINR}}^{(t)}$. In SDMA, such $\eta^{(t)}$ is a function of all UAVs since those within subset \mathcal{F}_k provide service while the rest create fronthaul interference. For the other two fronthaul strategies, only a subset of UAVs are relevant. To maintain a generic formulation, we derive the algorithm under SDMA fronthauling; minor changes apply for FDMA and FDMA-SDMA. The cost function can be expressed as $\eta^{(t)}(\ell_m^{(t)}, \forall m)$ and the 3D locations of the M UAVs are updated sequentially, starting with the lowest index.

Denote by $\mathcal{L}_{-m}^{(t)} = \{\boldsymbol{\ell}_1^{(t+1)}, \dots, \boldsymbol{\ell}_{m-1}^{(t+1)}, \boldsymbol{\ell}_{m+1}^{(t)}, \dots, \boldsymbol{\ell}_M^{(t)}\}$ the set of UAVs satisfying:

- a) UAVs $1, \ldots, m-1$ have already updated their locations to t+1;
- b) the locations of UAVs $m+1,\ldots,M$ still need to be updated; and
- c) UAV m is excluded.

The cost function allows an alternative expression as a function of $\mathcal{L}_{-m}^{(t)}$, namely $\eta^{(t)}(\boldsymbol{\ell}_m^{(t)}, \mathcal{L}_{-m}^{(t)})$. From [48], the probability of the mth UAV updating its 3D location to $\boldsymbol{\ell}_m^{(t+1)}$ is

$$\Pr\left\{\boldsymbol{\ell}_{m}^{(t+1)}|\boldsymbol{\ell}_{m}^{(t)},\boldsymbol{\mathcal{L}}_{-m}^{(t)}\right\} = \frac{\exp\left\{\gamma\,\eta^{(t)}\left(\boldsymbol{\ell}_{m}^{(t+1)},\boldsymbol{\mathcal{L}}_{-m}^{(t)}\right)\right\}}{\sum\limits_{\boldsymbol{\ell}_{m}^{(t+1)}\in\Theta^{t+1}} \exp\left\{\gamma\,\eta^{(t)}\left(\boldsymbol{\hat{\ell}}_{m}^{(t+1)},\boldsymbol{\mathcal{L}}_{-m}^{(t)}\right)\right\}},\tag{66}$$

where γ is a fixed parameter and Θ^{t+1} represents the possible locations that UAV m can explore at Iteration t+1. To reduce the search space, the number of such locations is limited to $|\Theta^{t+1}|=18$ (see Fig. 4). The options are to stay, move north, move south, move east, move west, and move in the direction of the gradient in (64), as well as the corresponding twelve locations at a higher and lower altitude. The search space is the set of 3D positions confined between some minimum and maximum altitudes, respectively H_{\min} and H_{\max} . And, after each iteration, matrix $M^{(s)}$ is updated. A summary of the process is included in Algorithm 1 where ϵ is a stopping parameter.

It is proved in [59] that, for large enough γ and $t \to \infty$, the solution for (66) converges to the optimal solution with probability 1.

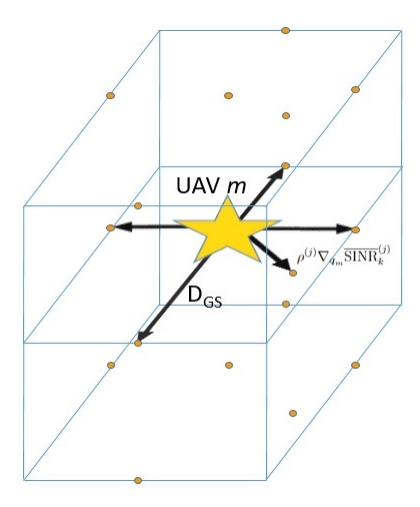


Fig. 4: 3D search space for UAV m with the dots representing Θ^{t+1} .

Algorithm 1 GS-GB Algorithm

```
Require: at t=0, initialize UAV locations, \ell_m^{(0)}, and cost function, \eta^{(0)} while \frac{|\eta^{(t+1)}-\eta^{(t)}|}{\eta^{(t)}}>\varepsilon do find the user with lowest cost function, k_{\min}^{(t)} for all m=1,\ldots,M do obtain \mathcal{L}_{-m,k_{\min}}^{(t)}. create the reduced search space with eighteen possible locations, \Theta^{t+1}. compute the cost function at the possible new locations, \eta^{(t)}(\hat{q}_m^{(t+1)},\mathcal{L}_{-m,k_{\min}}^{(t)}) for \hat{\ell}_m^{(t+1)}\in\Theta^{t+1}. calculate (66) and choose one movement accordingly, obtaining \ell_m^{(t+1)}. end for end while
```

VIII. NUMERICAL RESULTS

To evaluate the performance, we consider a 1 km^2 universe, wrapped around to avoid boundary effects. The simulation parameters are listed in Table I, selected based on the cell-free and UAV literature [27], [60]–[63]. Consistent with the neglect of pilot contamination, we consider $\tau = 200$ for a 3.2% pilot overhead. To ensure connectivity to multiple UAVs, the [m,k] entry of $M^{(s)}$ is 1 if $d_{k,m} \leq R_{\text{max}}$ for $R_{\text{max}} = 400$ m. The fading is IID, such that $\Omega_m = I$. Moreover, the noise arising in the fronthaul is scaled by a factor of M and L in SDMA and FDMA-

TABLE I: Simulation parameters

Description	Parameter	Value
Maximum transmit power	$p_{\mathrm{max}},\mathrm{p}_{\mathrm{max}}$	100 mW
Pathloss at 1 m	β_0	-30 dB
Pathloss exponent	κ	2.2
Dense urban parameters	A_1, A_2	0, 6.4 dB
Noise power for access and FDMA fronthaul	σ^2	-96 dBm
Antenna beamwidth	α_m	4
Operating frequency	$f_{ m c}$	2.4 GHz
Maximum UAV velocity	$v_{ m max}$	10 m/s
Coherence bandwidth	B_{c}	1 MHz
Number of UAVs	M	64
Number of users	K	45
Maximum and minimum altitude	$H_{\rm max},H_{ m min}$	25, 100 m

SDMA, respectively, to account for the bandwidth difference among the schemes. As for the GB-GS algorithm, and noting that other choices may be as effective, $\rho^{(t)} = T_{\rm GS} \cdot 1.005^{-t}$ where $T_{\rm GS}$ depends on the fronthaul scheme and is set to $T_{\rm GS} = 80$ for FDMA and to $T_{\rm GS} = 40$ for SDMA and FDMA-SDMA. In addition, $D_{\rm GS} = 1$ m (see Fig. 4) while $\gamma = 10$ and $\epsilon = 0.01$. The entries of $M^{(s)}$ are updated at every iteration of the GS-GB algorithm following the aforementioned distance-based rule with the frequency band allocations drawn at random. Finally, the user locations abide by a Poisson Point Process and the optimization algorithm that combines deployment and power optimization is tested over 100 deployments. When presenting results, the optimized deployment is denoted by A-O (after optimization) while a square grid UAV deployment, denoted by B-O (before optimization), serves as a benchmark.

We first evaluate the performance with FDMA fronthauling under a variety of parameters while validating the asymptotic derivations. Concretely, Fig. 5a plots the average per user spectral efficiency for different M and K. Additionally, Fig. 5b verifies Thm. 1 for different K/M. From Fig. 5b, a smaller K/M, i.e., more UAVs per ground user, provides better SINRs while allowing more UAVs to participate in the decoding of each user. Conversely, by looking at Fig. 5a, for fixed K, increasing M is not helpful in terms of spectral efficiency given the 1/M pre-log factor in (25). Finally, Fig. 5b shows that the derived results are indeed tight for finite-dimensional systems given the small gap between the $\mathbb{E}\{SINR\}$ and \overline{SINR} curves, with the advantage of only depending on large-scale parameters. A similar assessment is conducted for SDMA fronthauling

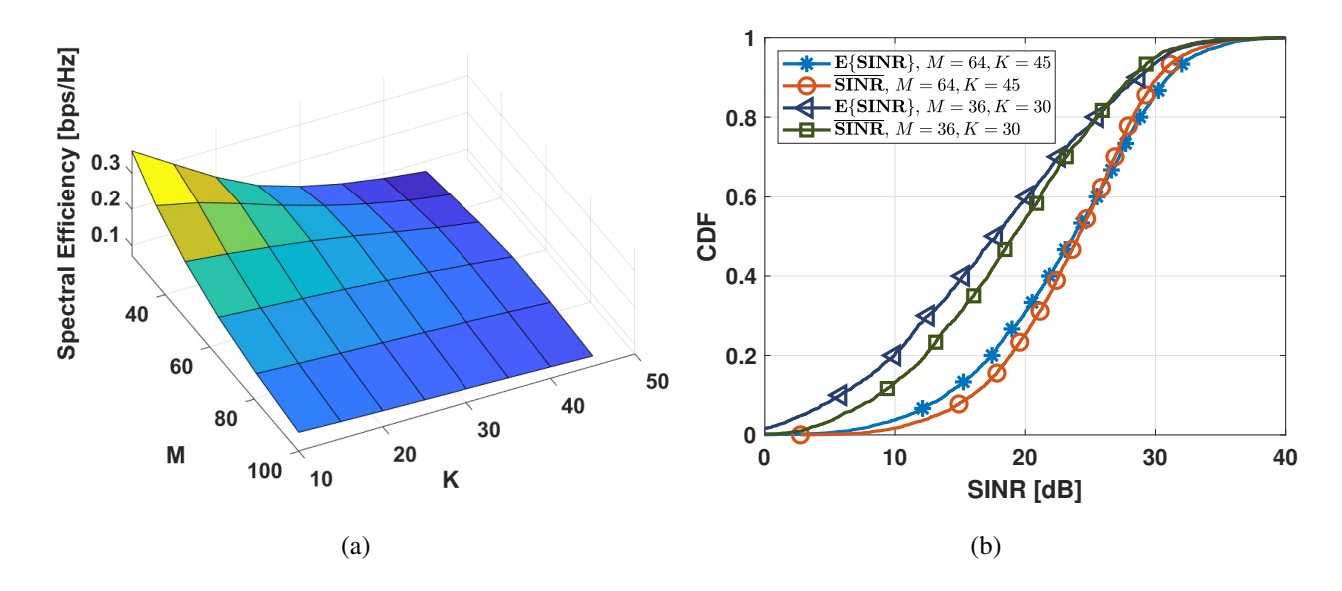


Fig. 5: (a) FDMA performance for different K, M; (b) validation of Thm. 1.

in Fig. 6. The number of antennas is set to N=1.2N. Interestingly, although SDMA provides lower SINRs compared to FDMA, an increase in M results in an improved spectral efficiency provided that the pre-log factor in Eq. (25) is one. This is because of the multiplexing gain in SDMA. Finally, Fig. 7 presents the results for FDMA-SDMA. We consider $L=\frac{M}{5}$ and N=1.2L, and the observations are consistent with those of FDMA and SDMA both in terms of (a) the tendency when varying the network load, and (b) the match between real and asymptotic SINR derivations.

As one would expect, the SINRs achieved with FDMA are decidedly higher because of the orthogonal nature of the transmisions and reduced noise bandwidth. In contrast (see Fig. 8), when measuring the sum spectral efficiency, SDMA vastly outperforms FDMA thanks to its spatial multiplexing gain. The hybrid FDMA-SDMA scheme balances the two.

Turning now to the deployment optimization, Fig. 9 presents results under FDMA fronthauling with different κ and α_m . Particularly, with the aim of keeping a small legend, the values shown in such figures are (κ, α_m) where B-O and A-O, recall, stand for before and after optimization, respectively. Specifically, Fig. 9a plots the B-O and A-O distributions; the optimization is highly effective, with at least 45% of users improving their SINR as a result. Then, Fig. 9b presents the CDF of the minimum SINR, where the optimization yields a 8-18 dB gain.

Fig. 10 presents results for the SDMA fronthaul parameterized by (κ, α_m) . For $\kappa = 2.2, 40$ -

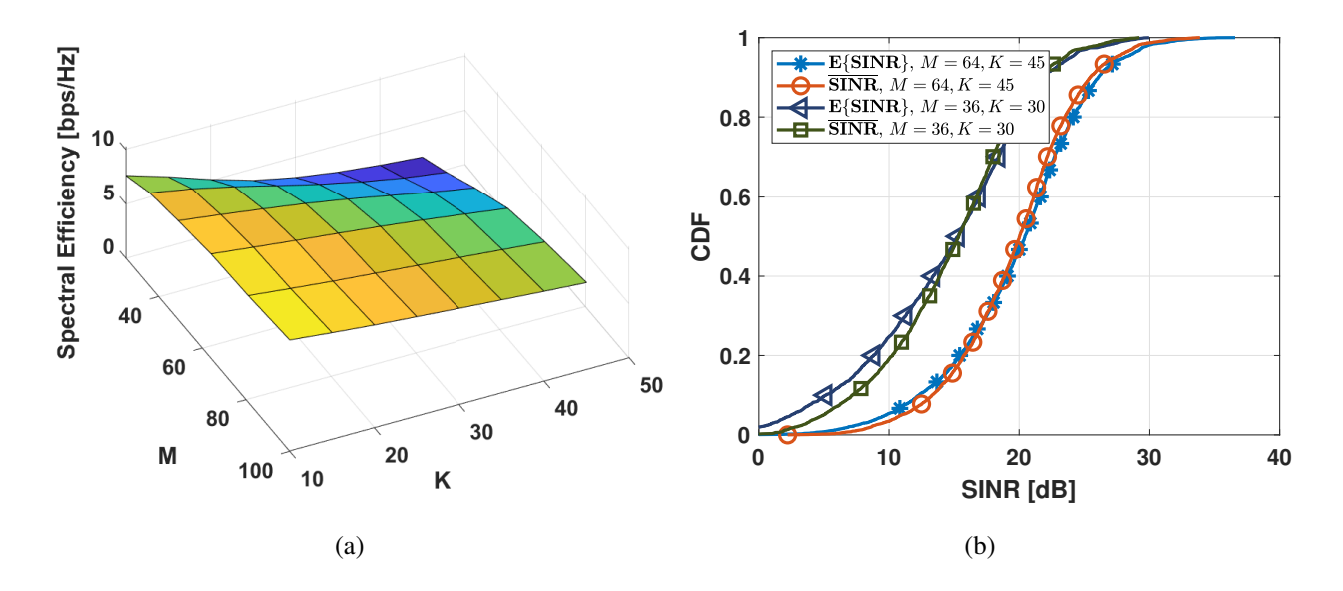


Fig. 6: (a) SDMA under different K, M; (b) validation of Thm. 3.

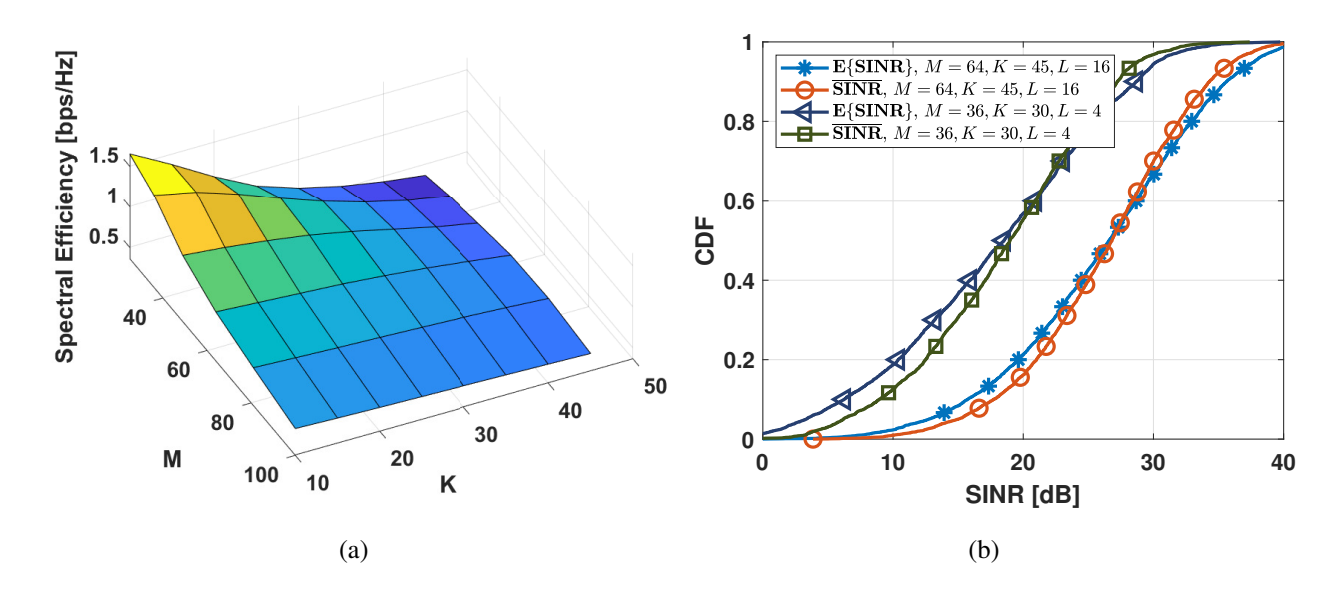


Fig. 7: (a) FDMA-SDMA for different $K, M, L = \frac{M}{5}$; (b) validation of Thm. 4.

60% of users enjoy an improved SINR after the optimization. For a higher pathloss exponent, $\kappa = 3$, it is 20-40%. The minimum SINR improves by 5-17 dBs for a variety of κ and α_m .

Results for the third fronthaul option, which combines FDMA and SDMA, are included in Fig. 11 for different (α_m , L, N). Again, the combination of deployment and power optimization highly increases the SINR experienced by those users with unfavorable initial conditions. Con-

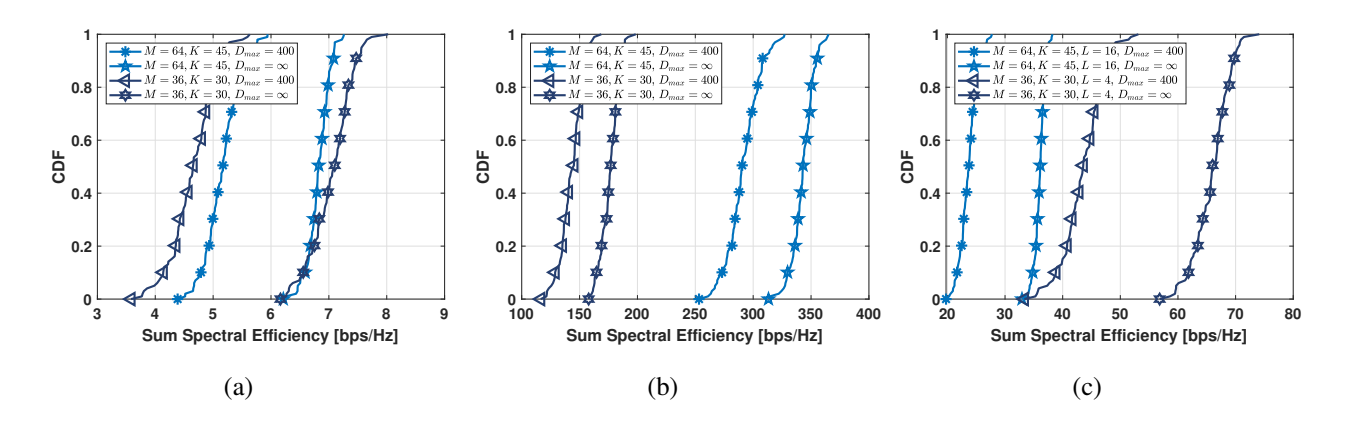


Fig. 8: Sum spectral efficiency under different network loads K/M for (a) FDMA; (b) SDMA; (c) FDMA-SDMA.

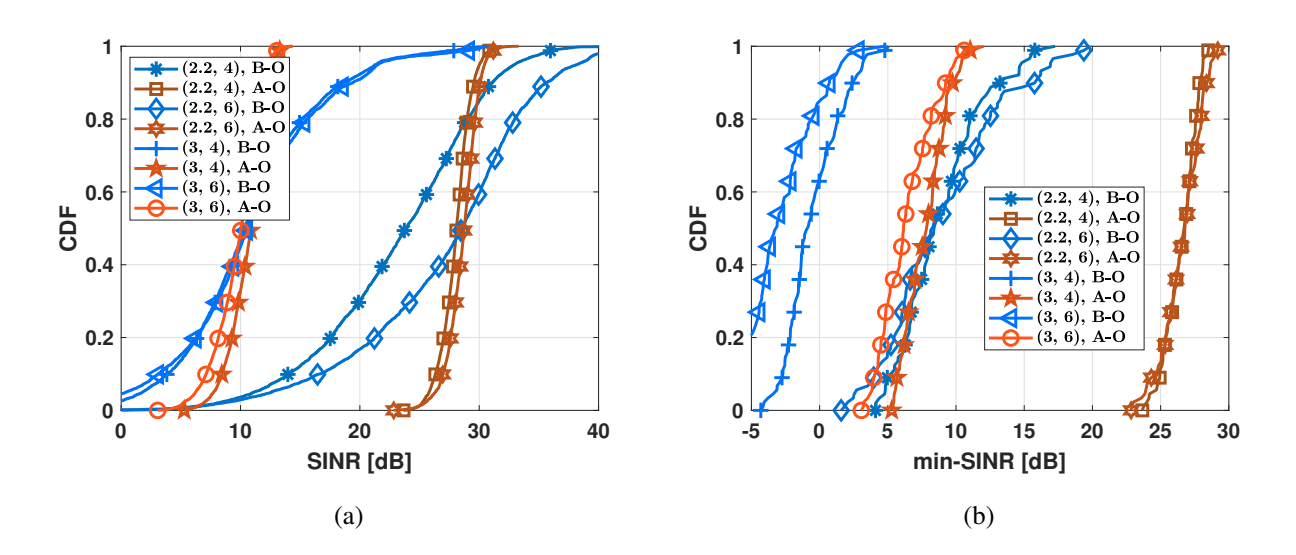


Fig. 9: CDFs B-O and A-O for different κ and α_m under an FDMA fronthaul (a) $\mathbb{E}\{SINR_k\}$; (b) min- $\mathbb{E}\{SINR_k\}$.

cretely, at least 50% of the SINRs are increased depending on the network parameters while the gains in terms of minimum SINR are 12-27 dB.

In Figs. 12a and 12b, respectively for FDMA and SDMA fronthauls, we provide insight on the contributions to the optimization gain. Precisely, we present the CDFs B-O, A-O, only optimizing the deployment (DEPLOY-O) and only optimizing the transmit powers (POWER-O) (POWER-O) for (a) FDMA; (b) SDMA. Power optimization helps to increase the lowest SINRs for 20-30% of users. However, the main source of gain is from the deployment optimization,

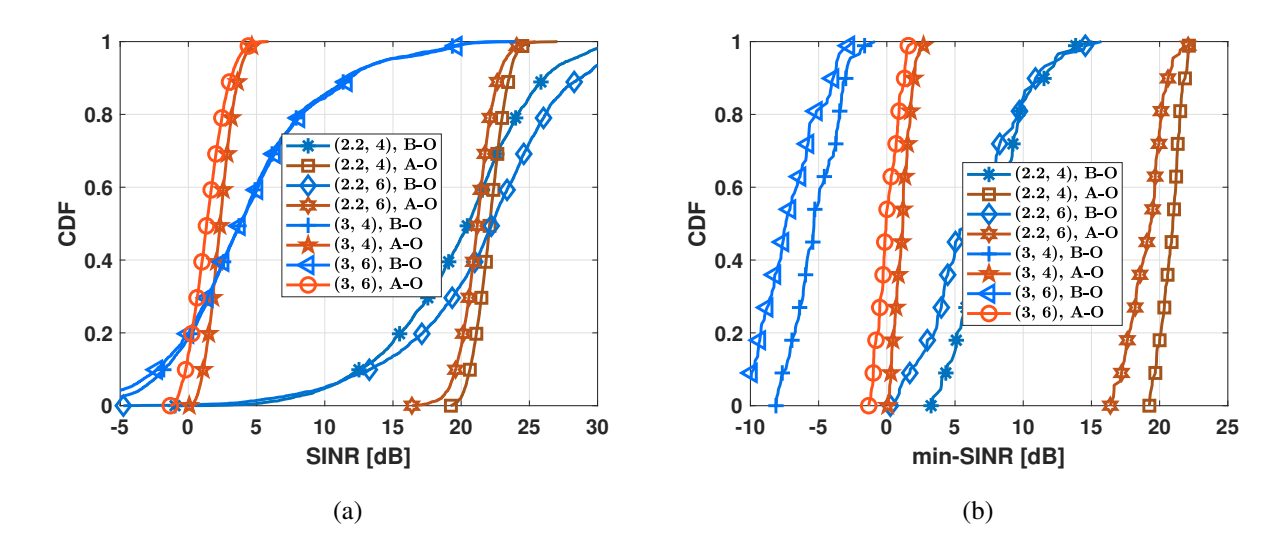


Fig. 10: CDF B-O and A-O parameterized by (κ, α_m) under SDMA fronthaul with N=80 (a) $\mathbb{E}\{SINR_k\}$; (b) $\min -\mathbb{E}\{SINR_k\}$.

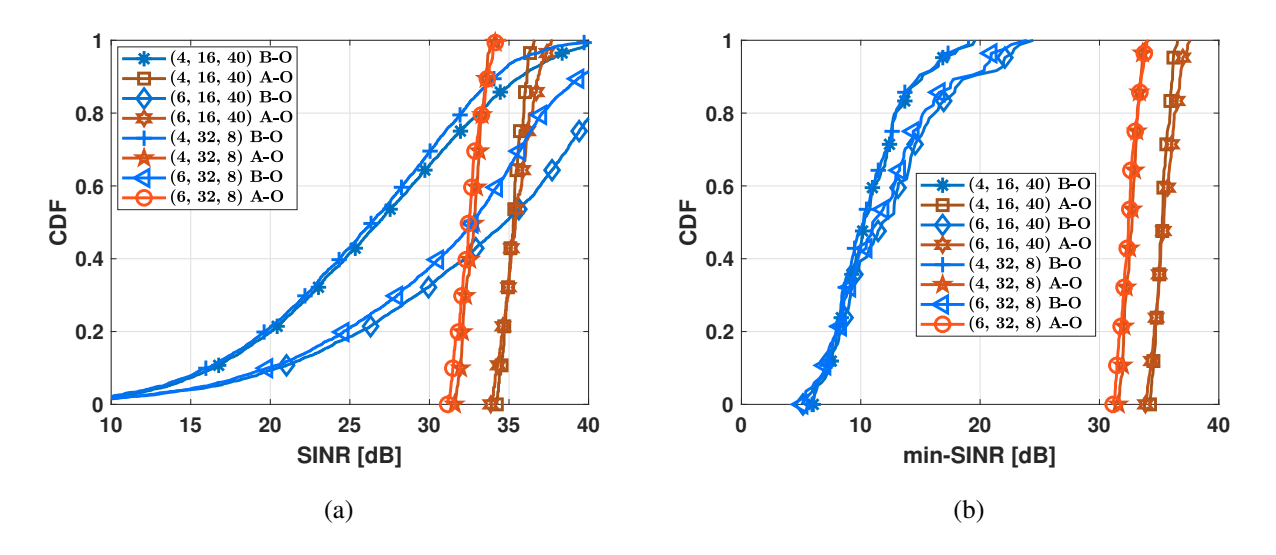


Fig. 11: CDF B-O and A-O parameterized by (α_m, L) and N under FDMA-SDMA fronthaul (a) $\mathbb{E}\{SINR_k\}$; (b) $\min -\mathbb{E}\{SINR_k\}$.

improving 90-100% of the user SINRs.

IX. CONCLUSION

This paper has considered a cell-free network with wireless access and fronthaul links. For the latter, a variety of schemes have been considered, namely FDMA, SDMA, and FDMA-

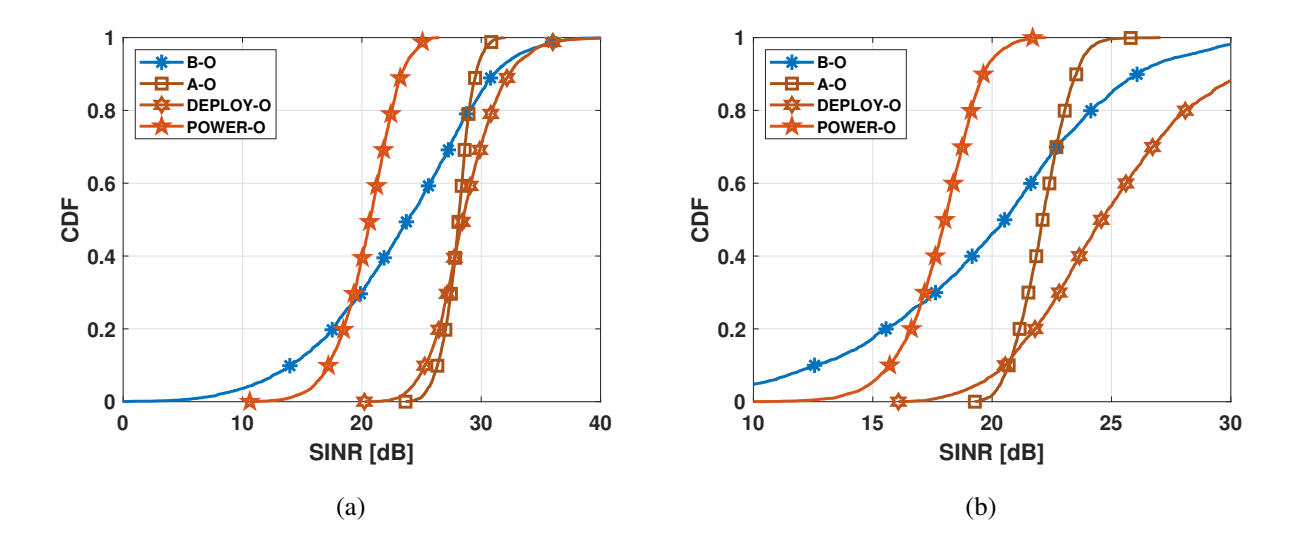


Fig. 12: $\mathbb{E}\{SINR_k\}$ CDF B-O, A-O, DEPLOY-O and POWER-O for $\kappa = 2.2$ and $\alpha_m = 4$ for (a) FDMA fronthaul; (b) SDMA fronthaul.

SDMA. Under Rician fading for the access and fronthaul links, deterministic equivalents for the SINR with MMSE reception have been provided for the three fronthaul schemes. Based on these deterministic expressions, the minimum SINR has been maximized with respect to (a) the 3D UAV locations, (b) user transmit power, and (c) UAV transmit power. A combination of gradient-based and Gibbs sampling algorithms has been employed for the former, and classic optimization techniques for the latter two.

Extensive results have shown how the optimization of the minimum SINR provides superior and fairer conditions in the network. Gains of 5-27 dB are achieved depending on the fronthaul techniques and network parameters. Further results have uncovered that the lion's share of the improvements can be attributed to the deployment optimization, with marginal additional gains associated with the optimization to the transmit powers.

APPENDIX A

Theorem 5. ([45, Thm. 1]) Let $\mathbf{D} \in \mathbb{C}^{M \times M}$ and $\mathbf{S} \in \mathbb{C}^{M \times M}$ be Hermitian nonnegative-definite while $\mathbf{H} \in \mathbb{C}^{M \times M}$ is a random matrix with zero-mean independent column vectors, \mathbf{h}_k , each with covariance matrix $\frac{1}{M}\mathbf{R}_k$. In turn, \mathbf{D} and \mathbf{R}_k have uniformly bounded spectral norm w.r.t. M. For z > 0 and $M, K \to \infty$,

$$\frac{1}{M}\operatorname{tr}\big[\boldsymbol{D}\big(\boldsymbol{H}\boldsymbol{H}^*+\boldsymbol{S}+z\boldsymbol{I}_M)^{-1}\big]-\frac{1}{M}\operatorname{tr}[\boldsymbol{D}\boldsymbol{T}]\overset{a.s.}{\to}0,$$

where

$$T = \left(\frac{1}{M} \sum_{j=1}^{K} \frac{\mathbf{R}_j}{1 + e_j} + \mathbf{S} + z \mathbf{I}_M\right)^{-1},\tag{67}$$

with coefficients $e_k = \lim_{n \to \infty} e_k^{(n)}$ for

$$e_k^{(n)} = \frac{1}{M} \operatorname{tr} \left[\mathbf{R}_k \left(\frac{1}{M} \sum_{j=1}^K \frac{\mathbf{R}_j}{1 + e_j^{(n-1)}} + \mathbf{S} + z \mathbf{I}_M \right)^{-1} \right],$$
 (68)

with initial values $e_k^{(0)} = M$.

APPENDIX B

Theorem 6. ([45, Thm. 2]) Let $\Phi \in \mathbb{C}^{M \times M}$ be Hermitian nonnegative-definite. Under the same conditions as Thm. 5, for $M, K \to \infty$,

$$\frac{1}{M}\operatorname{tr}\big[\boldsymbol{D}\big(\boldsymbol{H}\boldsymbol{H}^*+\boldsymbol{S}+z\boldsymbol{I}_M)^{-1}\boldsymbol{\Phi}\big(\boldsymbol{H}\boldsymbol{H}^*+\boldsymbol{S}+z\boldsymbol{I}_M)^{-1}\big]-\frac{1}{M}\operatorname{tr}\big[\boldsymbol{D}\boldsymbol{T}'(z,\boldsymbol{\Phi})\big]\overset{a.s.}{\to}0,$$

where $T'(z, \Phi)$ is defined as

$$T'(z, \mathbf{\Phi}) = T\mathbf{\Phi}T + T\frac{1}{M} \sum_{k=1}^{K} \frac{\mathbf{R}_k e_k'(z, \mathbf{\Phi})}{(1 + e_k)^2} T,$$
(69)

with T and e_k given in Thm. 5 for given z and $\mathbf{e}'(z, \mathbf{\Phi}) = \left(e_1'(z), \ldots, e_K'(z)\right)$ computed as

$$e'(z, \mathbf{\Phi}) = (\mathbf{I} - \mathbf{J}(z))^{-1} \mathbf{v}(z, \mathbf{\Phi}), \tag{70}$$

with $\mathbf{J}(z) \in \mathbb{C}^{K \times K}$ and $\mathbf{v}(z) \in \mathbb{C}^{K \times 1}$ defined as

$$\left(\boldsymbol{J}(z)\right)_{k,l} = \frac{\frac{1}{M} \operatorname{tr}\left[\boldsymbol{R}_k \boldsymbol{T} \boldsymbol{R}_l \boldsymbol{T}\right]}{M(1+e_l)^2},\tag{71}$$

and

$$(\boldsymbol{v}(z,\boldsymbol{\Phi}))_k = \frac{1}{M} \text{tr}[\boldsymbol{R}_k \boldsymbol{T} \boldsymbol{\Phi} \boldsymbol{T}].$$
 (72)

APPENDIX C

Define the matrix

$$\Omega_k = \left(\left(\boldsymbol{c}_k \circ \boldsymbol{M}^{(s)} \circ \hat{\boldsymbol{G}}_k \right) \boldsymbol{P} \left(\boldsymbol{c}_k \circ \boldsymbol{M}^{(s)} \circ \hat{\boldsymbol{G}}_k \right)^* - \left(\boldsymbol{c}_k \circ \hat{\boldsymbol{g}}_k \right) \left(\boldsymbol{c}_k \circ \hat{\boldsymbol{g}}_k \right)^* p_k + \Sigma_k \right)^{-1}, \quad (73)$$

where $P = \text{diag}\{p_k \,\forall \, k\}$ and $\Omega'_k = |\mathcal{F}_k|\Omega_k$. Then, (26) can be written as

$$SINR_k = (\boldsymbol{c}_k \circ \hat{\boldsymbol{g}}_k)^* \Omega_k (\boldsymbol{c}_k \circ \hat{\boldsymbol{g}}_k) p_k$$
(74)

$$= \frac{p_k}{|\mathcal{F}_k|} \operatorname{tr} \left[\left(\boldsymbol{c}_k \circ \hat{\boldsymbol{g}}_k \right) \left(\boldsymbol{c}_k \circ \hat{\boldsymbol{g}}_k \right)^* \Omega_k' \right]. \tag{75}$$

For $|\mathcal{F}_k|, |\mathcal{U}_m| \to \infty \ \forall \ k, m$, using [45, Lemma 4] and Thm. 5,

$$\frac{p_k}{|\mathcal{F}_k|}\operatorname{tr}\left[\left(\boldsymbol{c}_k\circ\hat{\boldsymbol{g}}_k\right)\left(\boldsymbol{c}_k\circ\hat{\boldsymbol{g}}_k\right)^*\boldsymbol{\Omega}_k'\right] - \frac{p_k}{|\mathcal{F}_k|}\operatorname{tr}\left[\boldsymbol{\Phi}\boldsymbol{\Gamma}_k\boldsymbol{T}_k\right] \stackrel{\text{a.s.}}{\to} 0. \tag{76}$$

In our case, the role of $(\boldsymbol{H}\boldsymbol{H}^*+\boldsymbol{S}+z\boldsymbol{I}_M)^{-1}$ in Thm. 5 is played by Ω_k' . There is a direct mapping between the terms in the aforementioned theorem and our problem, namely (i) $\boldsymbol{D} = \boldsymbol{\Phi}\boldsymbol{\Gamma}_k\,p_k$, (ii) $\boldsymbol{R}_j = \boldsymbol{\Phi}\boldsymbol{\Gamma}_j\,p_j$, and (iii) $\boldsymbol{S} + z\boldsymbol{I}_M = \frac{1}{|\mathcal{F}_k|}\boldsymbol{\Sigma}_k$ with matrix \boldsymbol{T}_k following the structure of \boldsymbol{T} in Thm. 5, namely

$$\boldsymbol{T}_{k} = \left(\frac{1}{|\mathcal{F}_{k}|} \sum_{j \neq k}^{K} \frac{\boldsymbol{\Phi} \boldsymbol{\Gamma}_{j}}{1 + e_{j}} p_{j} + \frac{1}{|\mathcal{F}_{k}|} \boldsymbol{\Sigma}_{k}\right)^{-1}.$$
 (77)

The necessary coefficients can be calculated as $e_j = \lim_{n \to \infty} e_j^{(n)}$ with

$$e_j^{(n)} = p_j \operatorname{tr} \left[\mathbf{\Phi} \mathbf{\Gamma}_j \left(\sum_{i \neq j}^K \frac{\mathbf{\Phi} \mathbf{\Gamma}_i}{1 + e_i^{(n-1)}} \, p_i + \mathbf{\Sigma}_j \right)^{-1} \right]. \tag{78}$$

The fixed-point algorithm can be used to compute $e_j^{(n)}$ and has been proved to converge [45]. Finally, since matrices Γ_k and T_k are diagonal, (76) can be written as

$$\frac{p_k}{|\mathcal{F}_k|} \operatorname{tr}[\boldsymbol{\Phi} \boldsymbol{\Gamma}_k \boldsymbol{T}_k] = p_k \operatorname{tr} \left[\boldsymbol{\Phi} \boldsymbol{\Gamma}_k \left(\sum_{i \neq k}^K \frac{\boldsymbol{\Phi} \boldsymbol{\Gamma}_i}{1 + e_i} p_i + \boldsymbol{\Sigma}_k \right)^{-1} \right], \tag{79}$$

and, with some straightforward algebra, the expression in Prop. 1 is obtained.

APPENDIX D

The definition of competitive utility functions and monotonic constraints are available at [56, Assumptions 1 and 2]. In our case, the utility function of user k is given in Thm. 1. It satisfies positivity because each $\overline{\text{SINR}}_{k,m}$ in (31) is positive. Then, to verify competitiveness, it is enough to show that a function of the type $\sum_{m \in \mathcal{F}_k} \frac{a_{k,m}p_k}{c_{k,m}+d_{k,m}p_k}$ is always increasing for $a_{k,m}, c_{k,m}, d_{k,m} > 0$. Indeed,

$$\frac{d}{d p_k} \sum_{m \in \mathcal{F}_k} \frac{a_{k,m} p_k}{c_{k,m} + d_{k,m} p_k} = \sum_{m \in \mathcal{F}_k} \frac{a_{k,m} c_{k,m}}{(c_{k,m} + d_{k,m} p_k)^2} > 0.$$
 (80)

Similarly, it can be shown that $\overline{\text{SINR}}_k$ is decreasing with respect to p_i for $i \neq k$. Finally, to show directional monotonicity, we substitute p_i by $\mu p_i \, \forall \, i$ and define the new SINR by $\overline{\text{SINR}}_k^{\mu}$. After some straightforward algebraic manipulations,

$$\overline{\text{SINR}}_{k}^{\mu} = \sum_{m \in \mathcal{F}_{k}} \frac{\gamma_{k,m} p_{k}}{\sum_{\substack{i \in \mathcal{U}_{m} \\ i \neq k}} \frac{\gamma_{i,m}}{1 + e_{i,k}} p_{i} + \frac{r_{m}}{\phi_{m}} \left(\sum_{\forall i} r_{i,m} p_{i} + \frac{\sigma^{2}}{\mu}\right) - \sum_{i \in \mathcal{U}_{m}} \gamma_{i,m} p_{i} + \frac{\sum_{i=1}^{K} r_{i} p_{i} + \frac{\sigma^{2}}{\mu}}{\phi_{m} p_{m}} \sigma^{2}}.$$
 (81)

All the terms in $\overline{\mathrm{SINR}}_k^\mu$ are as in $\overline{\mathrm{SINR}}_k$ except for the ones that depend on σ^2 , which are divided by μ . Provided that $\mu > 1$, each of the denominators is smaller in $\overline{\mathrm{SINR}}_k^\mu$ and thus $\overline{\mathrm{SINR}}_k^\mu \geq \overline{\mathrm{SINR}}_k$ for $\mu > 1$. Finally, it is easy to show that $p_k \leq p_{\mathrm{max}}$ are monotonic constraints.

APPENDIX E

Given a ZF fronthaul combiner U, we can make construct $U^{(\epsilon)} = \hat{H}(\hat{H}^*\hat{H} + \epsilon I)^{-1}$ satisfying $U = \lim_{\epsilon \to 0} U^{(\epsilon)}$. For ease of exposition, we define $\Omega = (\frac{1}{N}\hat{H}\hat{H}^* + \frac{\epsilon}{N}I)^{-1}$ while Ω_m equals Ω without the contribution of the mth channel. Note that $U^{(\epsilon)} = \frac{1}{N}\hat{H}\Omega$. In addition,

$$\boldsymbol{U}^{(\epsilon)} = \hat{\boldsymbol{H}}(\hat{\boldsymbol{H}}^* \hat{\boldsymbol{H}} + \epsilon \boldsymbol{I})^{-1} = (\hat{\boldsymbol{H}} \hat{\boldsymbol{H}}^* + \epsilon \boldsymbol{I})^{-1} \hat{\boldsymbol{H}} = \frac{1}{N} \Omega \hat{\boldsymbol{H}}.$$
 (82)

As a consequence, $\mathbb{E}\{oldsymbol{u}_m^{(\epsilon)*}oldsymbol{Q}oldsymbol{u}_m^{(\epsilon)}\}$ can be written as

$$\mathbb{E}\{\boldsymbol{u}_{m}^{(\epsilon)*}\boldsymbol{Q}\boldsymbol{u}_{m}^{(\epsilon)}\} = \mathbb{E}\left\{\frac{1}{N^{2}}\hat{\boldsymbol{h}}_{m}^{*}\boldsymbol{\Omega}\boldsymbol{Q}\boldsymbol{\Omega}\hat{\boldsymbol{h}}_{m}\right\}.$$
(83)

The term inside the expectation satisfies

$$\frac{1}{N^2}\hat{\boldsymbol{h}}_m^* \Omega \boldsymbol{Q} \Omega \hat{\boldsymbol{h}}_m = \frac{\frac{1}{N^2} \hat{\boldsymbol{h}}_m^* \Omega_m \boldsymbol{Q} \Omega_m \hat{\boldsymbol{h}}_m}{(1 + \frac{1}{N} \hat{\boldsymbol{h}}_m^* \Omega_m \hat{\boldsymbol{h}}_m)^2}$$
(84)

$$= \frac{N_m}{(1 + D_m)^2}. (85)$$

Note that N_m converges a.s. to

$$N_m \stackrel{\text{a.s.}}{\to} \frac{1}{N^2} \text{tr} \left(\Phi_m \Omega_m Q \Omega_m \right)$$
 (86)

$$\stackrel{\text{a.s.}}{\to} \frac{1}{N^2} \text{tr} \left(\Phi_m \mathbf{T}'(\epsilon, \mathbf{Q}) \right), \tag{87}$$

where $T'(\epsilon, Q)$ is provided in Thm. 6 for $D = \Phi_m$, $\Phi = Q$, S = 0, $z = \epsilon$, $R_k = \Phi_k$ and by substituting M = N. For the term in the denominator, applying Thm. 5,

$$D_m \stackrel{\text{a.s.}}{\to} \frac{1}{N} \text{tr} \left(\mathbf{\Phi}_m \mathbf{\Omega}_m \right) \tag{88}$$

$$\stackrel{\text{a.s.}}{\to} \frac{1}{N} \text{tr} \left(\mathbf{\Phi}_m \mathbf{T} \right), \tag{89}$$

where the same substitutions used to obtain $T'(\epsilon, Q)$ are made in Thm. 5 to acquire T. Applying the continuous mapping theorem,

$$\mathbb{E}\{\boldsymbol{u}_{m}^{(\epsilon)*}\boldsymbol{Q}\boldsymbol{u}_{m}^{(\epsilon)}\} - \frac{\frac{1}{N^{2}}\mathrm{tr}\left(\boldsymbol{\Phi}_{m}\boldsymbol{T}'(\epsilon,\boldsymbol{Q})\right)}{\left(1 + \frac{1}{N}\mathrm{tr}\left(\boldsymbol{\Phi}_{m}\boldsymbol{T}\right)\right)^{2}} \stackrel{\text{a.s.}}{\to} 0.$$
(90)

Taking the limit when $\epsilon \to 0$ in both terms results in the convergence stated in Thm. 2.

REFERENCES

- [1] W. Jiang, B. Han, M. A. Habibi, and H. D. Schotten, "The Road Towards 6G: A Comprehensive Survey," *IEEE Open Journal of the Commun. Soc.*, vol. 2, pp. 334–366, Feb. 2021.
- [2] J. Guo, P. Walk, and H. Jafarkhani, "Optimal Deployments of UAVs With Directional Antennas for a Power-Efficient Coverage," *IEEE Trans. Commun.*, vol. 68, pp. 5159–5174, Aug. 2020.
- [3] E. Koyuncu, M. Shabanighazikelayeh, and H. Seferoglu, "Deployment and Trajectory Optimization of UAVs: A Quantization Theory Approach," *IEEE Trans. on Wireless Commun.*, vol. 17, pp. 8531–8546, Dec. 2018.
- [4] C. Diaz-Vilor and H. Jafarkhani, "Optimal 3D-UAV Trajectory and Resource Allocation of DL UAV-GE Links with Directional Antennas," 2020 IEEE Global Commun. Conf., pp. 1–6, Dec. 2020.
- [5] J. Guo and H. Jafarkhani, "Movement-efficient sensor deployment in wireless sensor networks with limited communication range," *IEEE Transactions on Wireless Communications*, vol. 18, pp. 3469–3484, July 2019.
- [6] Y. Zeng, X. Xu, and R. Zhang, "Trajectory Design for Completion Time Minimization in UAV-Enabled Multicasting," *IEEE Trans. Wireless Commun.*, vol. 17, pp. 2233–2246, Apr. 2018.
- [7] Q. Wu, Y. Zeng, and R. Zhang, "Joint Trajectory and Communication Design for Multi-UAV Enabled Wireless Networks," *IEEE Trans. Wireless Commun.*, vol. 17, pp. 2109–2121, Mar. 2018.
- [8] J. Guo and H. Jafarkhani, "Sensor Deployment With Limited Communication Range in Homogeneous and Heterogeneous Wireless Sensor Networks," *IEEE Trans. on Wireless Commun.*, vol. 15, pp. 6771–6784, Oct. 2016.
- [9] C. You and R. Zhang, "3D Trajectory Optimization in Rician Fading for UAV-Enabled Data Harvesting," *IEEE Trans. Wireless Commun.*, vol. 18, pp. 3192–3207, Jun. 2019.
- [10] J. Guo, E. Koyuncu, and H. Jafarkhani, "A Source Coding Perspective on Node Deployment in Two-Tier Networks," *IEEE Trans. Commun.*, vol. 66, pp. 3035–3049, Jul. 2018.
- [11] F. Cheng, S. Zhang, Z. Li, Y. Chen, N. Zhao, F. R. Yu, and V. C. Leung, "UAV Trajectory Optimization for Data Offloading at the Edge of Multiple Cells," *IEEE Trans. Vehicular Technology*, vol. 67, pp. 6732–6736, Jul. 2018.
- [12] Y. Zeng and R. Zhang, "Energy-Efficient UAV Communication with Trajectory Optimization," *IEEE Trans. Wireless Commun.*, vol. 16, pp. 3747–3760, Jun. 2017.
- [13] Y. Zeng, J. Xu, and R. Zhang, "Energy Minimization for Wireless Communication with Rotary-Wing UAV," *IEEE Trans. Wireless Commun.*, vol. 18, pp. 2329–2345, Apr. 2019.
- [14] A. A. Khuwaja, Y. Chen, N. Zhao, M. S. Alouini, and P. Dobbins, "A Survey of Channel Modeling for UAV Communications," *IEEE Commun. Surveys and Tutorials*, vol. 20, pp. 2804–2821, Oct. 2018.
- [15] Y. Jing and H. Jafarkhani, "Network Beamforming Using Relays With Perfect Channel Information," *IEEE Trans. on Inf. Theory*, vol. 55, pp. 2499–2517, Jun. 2009.
- [16] Y. Jing and H. Jafarkhani, "Network Beamforming with Channel Means and Covariances at Relays," in 2008 IEEE International Conference on Communications, pp. 3743–3747, 2008.
- [17] D. Gesbert, S. Hanly, H. Huang, S. Shamai Shitz, O. Simeone, and W. Yu, "Multi-Cell MIMO Cooperative Networks: A New Look at Interference," *IEEE J. Sel. Areas in Commun.*, vol. 28, pp. 1380–1408, Dec. 2010.
- [18] E. Koyuncu and H. Jafarkhani, "Distributed Beamforming in Wireless Multiuser Relay-Interference Networks With Quantized Feedback," *IEEE Trans. Inf. Theory*, vol. 58, pp. 4538–4576, Jul. 2012.
- [19] Y.-W. Hong, W.-J. Huang, F.-H. Chiu, and C.-C. J. Kuo, "Cooperative Communications in Resource-Constrained Wireless Networks," *IEEE Sig. Process. Mag.*, vol. 24, pp. 47–57, May 2007.
- [20] J. Kazemitabar and H. Jafarkhani, "Performance Analysis of Multiple Antenna Multi-user Detection," in *Inf. Theory and Applications Workshop*, pp. 150–159, Jan. 2009.

- [21] G. Nigam, P. Minero, and M. Haenggi, "Coordinated Multipoint Joint Transmission in Heterogeneous Networks," *IEEE Trans. on Commun.*, vol. 62, pp. 4134–4146, Oct. 2014.
- [22] A. Checko, H. L. Christiansen, Y. Yan, L. Scolari, G. Kardaras, M. S. Berger, and L. Dittmann, "Cloud RAN for Mobile Networks—A Technology Overview," *IEEE Commun. Surveys Tutorials*, vol. 17, pp. 405–426, Sept. 2015.
- [23] J. Wu et al., "Cloud radio access network (C-RAN): a primer," IEEE Network, vol. 29, pp. 35-41, Jan. 2015.
- [24] P. Rost, C. J. Bernardos, A. D. Domenico, M. D. Girolamo, M. Lalam, A. Maeder, D. Sabella, and D. Wübben, "Cloud technologies for flexible 5G radio access networks," *IEEE Commun. Magazine*, vol. 52, pp. 68–76, Sept. 2014.
- [25] S. Venkatesan, A. Lozano, and R. Valenzuela, "Network MIMO: Overcoming intercell interference in indoor wireless systems," in *Asilomar Conf. on Signals, Systems and Computers*, pp. 83–87, 2007.
- [26] H. Q. Ngo, A. Ashikhmin, H. Yang, E. G. Larsson, and T. L. Marzetta, "Cell-Free Massive MIMO Versus Small Cells," *IEEE Trans. Wireless Commun.*, vol. 16, pp. 1834–1850, Mar. 2017.
- [27] H. Q. Ngo, L. Tran, T. Q. Duong, M. Matthaiou, and E. G. Larsson, "On the Total Energy Efficiency of Cell-Free Massive MIMO," *IEEE Trans. on Green Commun. and Net.*, vol. 2, pp. 25–39, Nov. 2018.
- [28] E. Björnson and L. Sanguinetti, "Making Cell-Free Massive MIMO Competitive With MMSE Processing and Centralized Implementation," *IEEE Trans. Wireless Commun.*, vol. 19, pp. 77–90, Jan. 2020.
- [29] M. Attarifar, A. Abbasfar, and A. Lozano, "Subset MMSE Receivers for Cell-Free Networks," *IEEE Trans. Wireless Commun.*, vol. 19, pp. 4183–4194, Jun. 2020.
- [30] R. Mosayebi, M. M. Mojahedian, and A. Lozano, "Linear Interference Cancellation for the Cell-Free C-RAN Uplink," IEEE Trans. on Wireless Commun., vol. 20, pp. 1544–1556, Nov. 2021.
- [31] G. Interdonato, P. Frenger, and E. G. Larsson, "Scalability Aspects of Cell-Free Massive MIMO," in 2019 IEEE Int'l Conf. on Commun. (ICC), pp. 1–6, May 2019.
- [32] E. Björnson and L. Sanguinetti, "Scalable Cell-Free Massive MIMO Systems," *IEEE Trans. on Commun.*, vol. 68, pp. 4247–4261, Jul. 2020.
- [33] M. Attarifar, A. Abbasfar, and A. Lozano, "Random vs structured pilot assignment in cell-free massive MIMO wireless networks," in *Int'l Conf. Commun. Workshops* (ICC Workshops), 2018.
- [34] C. D'Andrea *et al.*, "Analysis of UAV Communications in Cell-Free Massive MIMO Systems," *IEEE Open Journal of the Commun. Soc.*, vol. 1, pp. 133–147, Jan. 2020.
- [35] Ö. T. Demir and E. Björnson, "Joint power control and LSFD for wireless-powered cell-free massive MIMO," *IEEE Trans. on Wireless Commun.*, vol. 20, pp. 1756–1769, Mar. 2020.
- [36] O. Özdogan, E. Björnson, and J. Zhang, "Performance of cell-free massive MIMO with rician fading and phase shifts," *IEEE Trans. on Wireless Commun.*, vol. 18, pp. 5299–5315, Nov. 2019.
- [37] J. Zheng, J. Zhang, and B. Ai, "UAV communications with WPT-aided cell-free massive MIMO Systems," *IEEE J. Sel. Areas in Commun.*, pp. 1–1, Jan. 2021.
- [38] J. An and F. Zhao, "Trajectory optimization and power allocation algorithm in mbs-assisted cell-free massive MIMO systems," *IEEE Access*, vol. 9, pp. 30417–30425, 2021.
- [39] V. Tentu, E. Sharma, D. N. Amudala, and R. Budhiraja, "Uav-enabled hardware-impaired spatially correlated cell-free massive mimo systems: Analysis and energy efficiency optimization," *IEEE Trans. on Commun*, vol. 70, no. 4, pp. 2722– 2741, 2022.
- [40] C. Diaz-Vilor, A. Lozano, and H. Jafarkhani, "Cell-Free UAV Networks: Asymptotic Analysis and Deployment Optimization," *IEEE Trans. on Wireless Commun.*, pp. 1–1, Oct. 2022.
- [41] C. Diaz-Vilor, A. Lozano, and H. Jafarkhani, "On the deployment problem in Cell-Free UAV networks," in 2021 IEEE Global Commun. Conf. (GLOBECOM), Dec. 2021.

- [42] W. Hachem, M. Kharouf, J. Najim, and J. W. Silverstein, "A CLT for information-theoretic statistics of non-centered Gram random matrices," *Random Matrices: Theory and Applications*, vol. 1, no. 02, pp. 1–50, 2012.
- [43] W. Hachem, P. Loubaton, J. Najim, and P. Vallet, "On bilinear forms based on the resolvent of large random matrices," in *Annales de l'IHP Probabilités et statistiques*, vol. 49, pp. 36–63, 2013.
- [44] A. Kammoun, L. Sanguinetti, M. Debbah, and M.-S. Alouini, "Asymptotic Analysis of RZF in Large-Scale MU-MIMO Systems Over Rician Channels," *IEEE Trans. on Inf. Th.*, vol. 65, no. 11, pp. 7268–7286, 2019.
- [45] S. Wagner, R. Couillet, M. Debbah, and D. T. M. Slock, "Large System Analysis of Linear Precoding in Correlated MISO Broadcast Channels Under Limited Feedback," *IEEE Trans. on Inf. Th.*, vol. 58, pp. 4509–4537, Mar. 2012.
- [46] J. Hoydis, S. ten Brink, and M. Debbah, "Massive MIMO in the UL/DL of Cellular Networks: How Many Antennas Do We Need?," *IEEE J. on Sel. Areas in Commun.*, vol. 31, pp. 160–171, Feb. 2013.
- [47] B. Wang, J. Zhang, and A. Host-Madsen, "On the capacity of MIMO relay channels," *IEEE Trans. Inform. theory*, vol. 51, no. 1, pp. 29–43, 2005.
- [48] P. Bremaud, Markov Chains: Gibbs Fields, Monte Carlo Simulation, and Queues, vol. 31. Springer, 1999.
- [49] R. W. Heath Jr. and A. Lozano, Foundations of MIMO communication. Cambridge University Press, 2019.
- [50] S. Shimamoto and Iskandar, "Channel characterization and performance evaluation of mobile communication employing stratospheric platforms," *IEICE Trans. Commun.*, vol. E89-B, pp. 937–944, Mar. 2006.
- [51] C. A. Balanis, Antenna Theory: Analysis and Design. Wiley, 4th ed., 2016.
- [52] X. Wang, J. Cheng, C. Zhai, and A. Ashikhmin, "Partial cooperative zero-forcing decoding for uplink cell-free massive MIMO," *IEEE Internet of Things Journal*, vol. 9, pp. 10327–10339, Oct. 2022.
- [53] X. Wang, A. Ashikhmin, Z. Dong, and C. Zhai, "Two-stage channel estimation approach for cell-free iot with massive random access," *IEEE J. on Sel. Areas in Commun.*, vol. 40, pp. 1428–1440, Jan. 2022.
- [54] A. Lozano, "Interplay of spectral efficiency, power and Doppler spectrum for reference-signal-assisted wireless communication," *IEEE Trans. Wireless Commun.*, vol. 7, no. 12, pp. 5020–5029, 2008.
- [55] H. B. Mann and A. Wald, "On Stochastic Limit and Order Relationships," Annals of Mathematical Statistics, vol. 14, pp. 217–226, 1943.
- [56] L. Zheng *et al.*, "Wireless Max–Min Utility Fairness With General Monotonic Constraints by Perron–Frobenius Theory," *IEEE Trans. on Information Th.*, vol. 62, pp. 7283–7298, Dec. 2016.
- [57] M. Diehl, F. Glineur, E. Jarlebring, and W. Michiels, *Recent Advances in optimization and its applications in engineering*. Springer Berlin Heidelberg, 2010.
- [58] S. P. Boyd and L. Vandenberghe, Convex optimization. Cambridge University Press, 2004.
- [59] L. P. Qian, Y. J. A. Zhang, and M. Chiang, "Distributed Nonconvex Power Control using Gibbs Sampling," *IEEE Trans. on Commun.*, vol. 60, pp. 3886–3898, Dec. 2012.
- [60] M. Mozaffari, W. Saad, M. Bennis, and M. Debbah, "Unmanned Aerial Vehicle With Underlaid Device-to-Device Communications: Performance and Tradeoffs," *IEEE Trans. Wireless Commun.*, vol. 15, pp. 3949–3963, Jun. 2016.
- [61] P. Chandhar, D. Danev, and E. G. Larsson, "Massive MIMO for Communications With Drone Swarms," *IEEE Trans. on Wireless Commun.*, vol. 17, pp. 1604–1629, March 2018.
- [62] "Enhanced LTE support for aerial vehicles," Tech. Rep. 36.777, 3GPP, Dec. 2017.
- [63] A. Al-Hourani and K. Gomez, "Modeling Cellular-to-UAV Path-Loss for Suburban Environments," *IEEE Wireless Commun. Lett.*, vol. 7, no. Jan., pp. 82–85, 2018.